Climate Dynamics (2026) 64:26
https://doi.org/10.1007/s00382-025-08009-8

Model-based exploration of the seasonal influences of lakes on glacier behavior over the Tibetan Plateau

Dongsheng Su[1] · Lijuan Wen[1,2,3] · Anning Huang[4] · Yang Wu[5] · Maoshan Li[1] · Zhiqiang Lin[1] · Xianyu Yang[1] · Dongnan Jian[1] · Georgiy Kirillin[6]

Received: 14 February 2025 / Accepted: 30 November 2025

Abstract
Glaciers on the Tibetan Plateau (TP) are retreating rapidly in response to global warming. While extensive research has focused on the spatial heterogeneity of glacier retreat across the TP, only a few studies have examined the role of TP lakes in shaping these patterns. In this study, we applied the Weather Research and Forecasting (WRF) model, coupled with a one-dimensional lake mass and energy balance scheme, to examine how TP lakes affect seasonal surface air temperature, snowfall, and water vapor flux, and how these lake-induced climatic changes influence the spatial heterogeneity and seasonal variability of glacier retreat across the region. Results show that TP lakes tend to reduce 2-m air temperature (T_{2m}) in glacierized regions in many seasons, and are associated with increased snowfall on some alpine glaciers in the Inner TP during summer and autumn, and on marginal glaciers during winter and spring. Furthermore, the seasonal climate effects of individual lakes vary regionally, and they may exert distinct influences on adjacent glaciers, particularly in autumn in our simulations. Langa Co and Mapam Yumco may contribute to reduced T_{2m} and enhanced snowfall over the Naimona'nyi Glacier to the south, which is consistent with the relatively slower retreat observed among glaciers in the West Himalayas. Similarly, Yamzho Yumco and Puma Yumco have comparable impacts on the Qiangyong Glacier in the Central Himalayas. Additionally, Nam Co exerts contrasting influences on the western Nyainqentanglha Range, mitigating glacier retreat on the southern slopes but intensifying it on the northern slopes during summer, with the opposite pattern occurring in autumn. Simulations indicate that TP lakes can modify regional moisture pathways, contributing to enhanced northward water vapor fluxes associated with the Indian Summer Monsoon in some cases, which may influence snowfall and glacier mass balance in regions such as the West Kunlun and Tanggula Mountains.

Keywords Tibetan Plateau · Lakes · Climatic effect · Glaciers · Numerical simulation

✉ Lijuan Wen
wlj@lzb.ac.cn

[1] Climate Change and Resource Utilization in Complex Terrain Regions Key Laboratory of Sichuan Province, Plain Urban Meteorology and Environment Observation and Research Station of Sichuan Province, Sichuan Provincial Engineering Research Center for Meteorological Disaster Prediction and Early Warning, School of Atmospheric Sciences, Chengdu University of Information Technology, Chengdu 610225, Sichuan, China

[2] State Key Laboratory of Cryospheric Science and Frozen Soil Engineering, Northwest Institute of Eco-Environment and Resources, Chinese Academy of Sciences, Lanzhou 730000, China

[3] Qinghai Lake Comprehensive Observation and Research Station, Chinese Academy of Sciences, Gangcha, China

[4] School of Atmospheric Sciences, Nanjing University, Nanjing 210023, China

[5] Nanjing Innovation Institute for Atmospheric Sciences, Chinese Academy of Meteorological Sciences-Jiangsu Meteorological Service, Nanjing, China

[6] Department of Ecohydrology, Leibniz-Institute of Freshwater Ecology and Inland Fisheries, 12587 Berlin, Germany

Published online: 22 December 2025

1 Introduction

The Tibetan Plateau (TP), with an average elevation exceeding 4000 m above sea level (a.s.l.), is often referred to as the Earth's Third Pole (Qiu 2008). It contains approximately 100,000 km^2 of glaciers, making it the largest cryospheric region outside the Antarctic and Arctic (Yao et al. 2019). Additionally, the TP is home to more than 1400 lakes (> 1 km^2), covering a total area of $5.0 \times 10^4 \pm 791.4$ km^2, which accounts for 57.2% of the total area of lakes in China (Zhang et al. 2019), and is thus also referred to as the "Asian Water Tower". These glaciers and lakes provide source water for 10 major Asian river systems, including the Yangtze, Yellow, Brahmaputra, Ganges, and Indus, supporting ~ 1.4 billion people across 10 downstream countries (Immerzeel et al. 2020; Miao et al. 2024).

Glaciers are highly sensitive to climate change. As global warming persists, TP glaciers have undergone continuous shrinkage and mass loss, accelerating in recent decades (Hugonnet et al. 2021; Miles et al. 2021; Su et al. 2022a). Glacier mass loss could result in a reduction or even disappearance of meltwater runoff in the future (Huss and Hock 2018), accompanied by various glacier-related hazards, such as surging, collapse, and glacial lake outburst flood (Gilbert et al. 2018; Kääb et al. 2018). Due to a positive feedback mechanism, glacier ablation at high elevations may exacerbate warming on the TP, which, in turn, further accelerates glacier melt (Zhang et al. 2022). Moreover, glacier changes on the TP exhibit distinct regional characteristics, with shrinkage generally increasing from the interior to the margins (Yang et al. 2019). This phenomenon is exemplified by the "Karakoram anomaly", with glaciers in the West Kunlun, Karakoram, and the Pamir Mountains experiencing minimal shrinkage or even slight growth (Farinotti et al. 2020; Hewitt 2005), while the southeastern TP seeing glacial retreat and mass loss approximately three times greater than the average rate over the entire plateau (Brun et al. 2017; Zhao et al. 2022a).

Glacier mass balance is primarily governed by interactions among the glacier surface, atmosphere, and snow cover, with air temperature and snowfall representing the two most critical meteorological drivers (van Angelen et al. 2013; van Pelt et al. 2016). While a substantial rise in air temperature is widely regarded as the primary cause of glacier shrinkage, growing emphasis has been placed on understanding the pronounced spatiotemporal heterogeneity of glacier changes across the TP (Chen et al. 2017; Wang et al. 2020). Previous studies have suggested that the weakened Indian Summer Monsoon and the strengthened mid-latitude westerlies play a crucial role in the spatiotemporal heterogeneity of glacial mass balance, by reducing precipitation over the Himalayas while increasing it over the Inner TP and the Pamir (Yang et al. 2014; Yao et al. 2022, 2012b). The seasonal interaction between the Karakoram vortex and the South Asian Monsoon also contributes to glacier changes in the Karakoram and western TP by modulating regional air temperature and precipitation patterns (Forsythe et al. 2017; Li et al. 2018). Other contributing factors to the spatial pattern of glacier changes include warming rates and shifts in monsoon precipitation phases (Farinotti et al. 2020; Hugonnet et al. 2021; Jouberton et al. 2022; Sakai and Fujita 2017). Furthermore, glacier morphology, such as size, debris coverage, elevation, slope, and aspect, also influences the spatiotemporal patterns of glacier changes (Maussion et al. 2014; Yu et al. 2013; Zhu et al. 2017).

In addition to external large-scale circulation, regional climatic effects induced by internal multi-sphere (atmosphere, cryosphere, hydrosphere, etc.) interactions represent another crucial factor influencing glacier behavior on the TP (Yao et al. 2012a). For instance, irrigation in the lowlands surrounding the TP, which increases snowfall and decreases net radiation, can promote summer glacier growth along the Kunlun Mountains and Pamir (de Kok et al. 2018). Due to the low sensitivity of glaciers to air temperature changes in the West Kunlun and Karakoram ranges, an increase in snowfall resulting from additional evapotranspiration due to irrigation can lead to positive mass balances in glaciers (de Kok et al. 2020). Despite considerable efforts to investigate the local climate effects of TP lakes in recent years (Dai et al. 2018; Li et al. 2017; Su et al. 2020; Wen et al. 2015; Zhao et al. 2022b), their climatic impacts on glacier behavior have received limited attention. Recent studies have shown that the TP lake cluster can significantly decrease air temperature and increase precipitation during the summer (Wu et al. 2019), probably contributing to a slower retreat rate of glaciers in the Inner TP compared to other regions on the plateau (Su et al. 2022b). However, the simulations in these studies only cover the summer, leaving the climatic impacts of lakes on glacier behavior in other seasons and their seasonal differences unexplored.

This study aims to investigate the seasonal contributions of TP lakes to the spatiotemporal patterns of glacier changes across the entire TP. To achieve this, we employed an air-lake coupled regional climate model to estimate the climatic effects of TP lakes, and divided TP glaciers into six subregions based on previous studies (Su et al. 2022b; Yao et al. 2012b), to facilitate a more comprehensive analysis. Our results enhance the understanding of the climatic impacts of multi-sphere interactions on glacier behavior and the factors contributing to the spatiotemporal heterogeneity of glacier changes on the TP.

2 Data and methods

2.1 Data

In-situ lake surface water temperature (LSWT) observations were obtained from a fixed platform at the China Torpedo Qinghai Lake Test Base (36°35′27.65″ N, 100°30′06″ E, 3,198 m a.s.l.), located ~ 737 m from the southeastern shore above 15 m water depth. An infrared thermometer (model SI-111, Campbell Scientific Inc.) mounted ~ 10 m above the lake surface recorded LSWT at high temporal resolution. These observations were used to validate the WRF-Lake model's ability to reproduce the seasonal evolution of LSWT at Qinghai Lake (Li et al. 2016).

The C3S_LSWT L3S v4.5.1 dataset, supplied by the Copernicus Climate Change Service (C3S) Lake production system, was utilized to validate the simulated LSWT. This dataset, essential for climate change research and monitoring, originates from the Global Observatory of Lake Responses to Environmental Changes (GloboLakes) data product (Politi et al. 2016). Based on the foundational work of the European Space Agency's Climate Change Initiative (ESA CCI) Lakes project, the C3S_LSWT v4.5 dataset synthesizes data from multiple satellite platforms, including ATSR2, AATSR, MODIS, AVHRR, and SLSTR. This comprehensive dataset provides daily global LSWT records for over 2,000 lakes at a spatial resolution of approximately 0.05°, supporting detailed environmental analysis. The dataset employs an Optimal Estimation (OE) algorithm to derive water temperatures from satellite-derived reflectance and brightness temperature data. It includes sophisticated pixel classification processes to distinguish water from non-water areas, accounts for cloud cover, and applies cross-sensor adjustments to ensure data integrity and consistency across observational sources.

The ERA5-Land hourly dataset was employed to evaluate the 2-m air temperature simulation. ERA5-Land is an advanced global land surface reanalysis dataset developed by the European Centre for Medium-Range Weather Forecasts (ECMWF). The dataset is derived from the land component of the ERA5 climate reanalysis, which is driven by meteorological fields from ERA5 at an enhanced resolution of 9 km, compared to 31 km in ERA5, allowing for a more accurate representation of small-scale features and processes over land. The dataset spans from January 1950 to approximately 2–3 months before the current date (Muñoz-Sabater et al. 2021).

The Global Precipitation Measurement (GPM) Integrated Multi-satellite Retrievals (IMERG) V06 Level 3 Final Daily Precipitation Product (GPM_3IMERGDF), with gauge adjustments, was employed to validate the simulated precipitation. This product is a state-of-the-art dataset designed to provide comprehensive and accurate precipitation measurements, with a spatial resolution of 0.1° × 0.1° for regions between 60°S and 60°N globally. The IMERG algorithm integrates precipitation estimates from various sources, including multi-satellite data with passive microwave (PMW) and infrared (IR) sensors. The IMERG-Final product is generated after incorporating both forward and backward morphing, along with monthly gauge analysis (Li et al. 2021).

ERA-Interim was employed to define the initial and boundary conditions for the Weather Research and Forecasting Model (WRF). ERA-Interim, a global atmospheric reanalysis developed by the European Centre for Medium-Range Weather Forecasts (ECMWF), employs the Integrated Forecast System (IFS) version 31r1 with a spatial resolution of approximately 80 km (T255), providing analyses at 00:00, 06:00, 12:00, and 18:00 UTC. This reanalysis spans from 1 January 1979 to 31 August 2019. ERA-Interim aims to precisely and reliably represent climate conditions by assimilating observational data and model forecasts (Dee et al. 2011).

2.2 Model description and experimental design

This study employed the Advanced Research Weather Research and Forecasting (WRF) model version 3.9.1 (Skamarock et al. 2008), a fully compressible and non-hydrostatic model that incorporates multiple parameterizations of sub-grid processes and land surface models. The physical parameterization schemes used in this study include the single-moment 6-class scheme (Hong and Lim 2006), the Noah land surface model (Chen and Dudhia 2001), the Grell-Devenyi ensemble cumulus scheme (Grell and Devenyi 2002), the Yonsei University planetary boundary layer (PBL) parameterization (Hong et al. 2006), the Dudhia shortwave radiation scheme (Dudhia 1989), and the Rapid Radiative Transfer Model (RRTM) longwave radiation scheme (Mlawer et al. 1997). In this study, the Noah land surface model was used to represent land–atmosphere interactions. Although the model does not simulate dynamic glacier mass balance or flow, glacierized surfaces are represented as static snow or ice-covered land grid cells with prescribed physical properties (e.g., high albedo and low heat capacity). This configuration allows for the evaluation of lake-induced climatic impacts, such as variations in temperature and snowfall, on glacier-relevant surface conditions. Within the WRF model, a lake scheme derived from the Community Land Model version 4.5 (CLM4.5) was incorporated to simulate lake thermal processes and their interactions with the atmosphere. This lake model is a one-dimensional (1-D) mass and energy balance model that evolved from a parameterization scheme developed by Hostetler et al. (1993) and

subsequently refined and validated by Subin et al. (2012) and Gu et al. (2015). It represents each lake grid cell using 25 horizontal layers: 10 layers for lake water and ice, 10 layers for bottom sediment, and 5 layers for snow overlying the lake ice. The model solves the vertical heat diffusion equation across all layers to simulate temperature profiles and phase changes. The lake scheme was activated in both nested domains (Domain 1 and Domain 2), ensuring consistent representation of lake-atmosphere interactions across spatial scales.

To study the climatic effects of the TP lakes and their potential influence on glaciers, two numerical experiments were conducted for comparison based on methodologies used in previous studies (Thiery et al. 2015; Wen et al. 2015; Wu et al. 2019; Zhu et al. 2020). The control (CTL) experiment employs the air-lake coupled WRF model for simulations with TP lakes. In contrast, the sensitive (SEN) experiment replaces the lakes with surrounding land cover, predominantly grassland, open shrublands, and barren or sparsely vegetated areas. The simulation began on 20 May 2013 and ended on 31 August 2014, with a 12-day model spin-up period.

The simulation employs a two-nested domain configuration with two-way interactions. As shown in Fig. 1, the outer domain (Domain 1) has a 30 km horizontal resolution, covering a substantial portion of the Asian continent, the northern part of the Indian Ocean, and part of the northwestern Pacific Ocean. This extensive geographical coverage is critical for capturing the impacts of the summer monsoon on moisture transport dynamics and atmospheric circulation within the simulation. The inner domain (Domain 2) has a higher resolution of 10 km and is centered over the southern region of the Inner TP, offering detailed coverage of nearly the entire TP. This localized focus, within the broader context of the outer domain, enables a nuanced examination of local meteorological phenomena influenced by larger climatic interactions. The domain configuration was designed to balance computational feasibility with optimal coverage

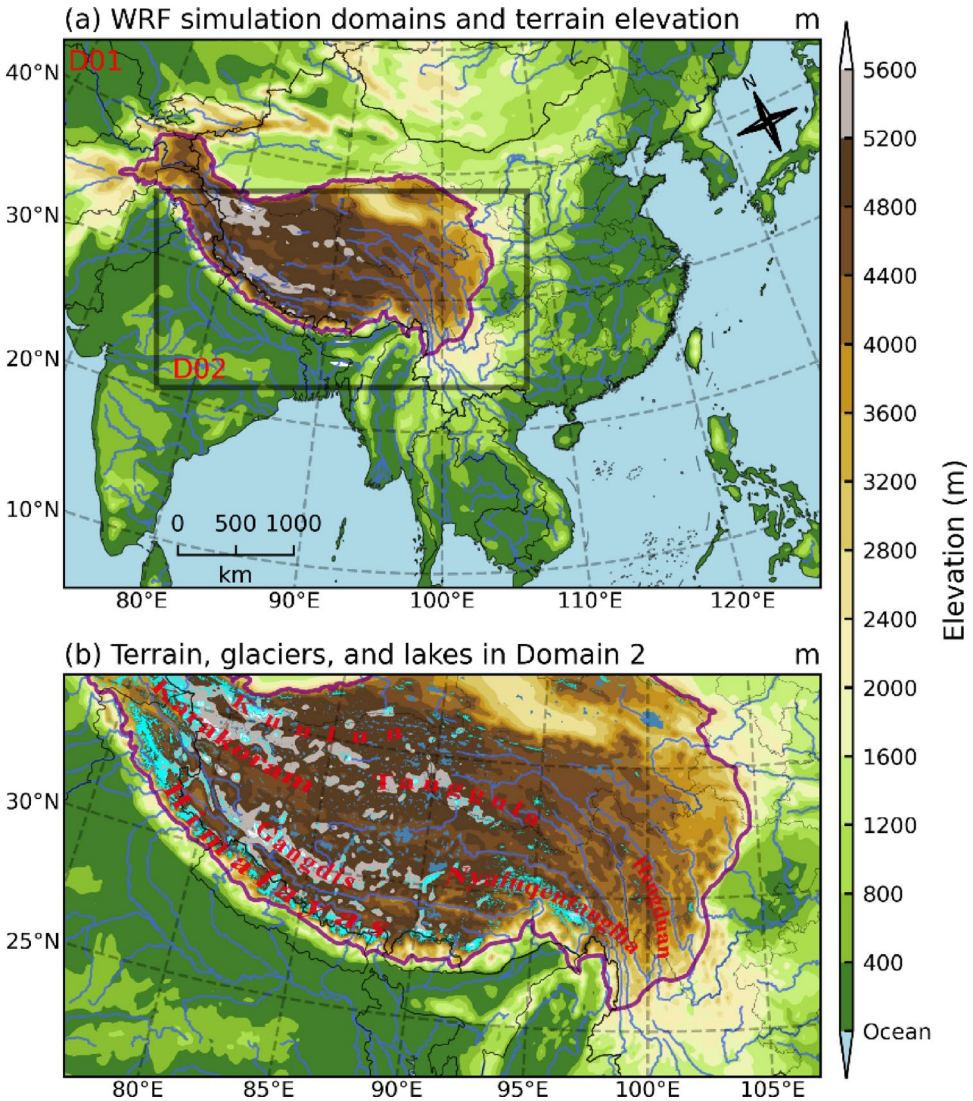

Fig. 1 **a** Geographic location and terrain elevation of the two nested domains used in the WRF model. **b** Distribution of terrain elevation, glaciers, and lakes in Domain 2. The purple line outlines the boundary of the TP, defined as areas above 3000 m elevation, and the royal blue lines represent major rivers. Lakes and glaciers are shown as steel blue and cyan areas, respectively

of dominant moisture pathways and lake-glacier interaction zones. Glacier areas analyzed in this study, particularly those located in the high-altitude western and central plateau, are situated well within the dynamically stable interior of Domain 2, sufficiently distant from lateral boundaries to minimize potential interference from relaxation zones. This ensures that simulated lake-induced thermal and dynamic processes over these key glacier regions are physically robust and minimally influenced by boundary effects. The initial and lateral boundary conditions were obtained from ERA-Interim reanalysis with a 6-h interval. Sea surface temperature was updated using the daily real-time global sea surface temperature dataset (Thiebaux et al. 2003).

To comprehensively assess the influence of the TP lakes on glaciers, the study area was divided into six subregions based on geographic location, climatic background, and lake-induced summer climate effects, following previous studies (Yao et al. 2012b). The glaciers assigned to each subregion, along with their key characteristics and changes in length over recent decades, are summarized in Table 1. Glaciers in the southern periphery of the TP (subregions 1, 2, and 3), primarily influenced by the Indian monsoon, have experienced the most pronounced retreat, particularly in subregion 3 (southeastern TP). In contrast, glaciers in the Inner TP (subregions 4 and 5) exhibit slower retreat rates, while those in the West Kunlun Mountains (subregion 6) show the least change. As most TP lakes are located in the Inner TP, their climatic influence is most pronounced in subregions 4 and 5 and relatively weak in peripheral regions. This subregional framework allows for a more detailed evaluation of glacier responses to lake-climate interactions across different climatic regimes.

2.3 Evaluation methodology

To evaluate model performance, several common statistical methods were employed, including BIAS, spatial root-mean-square error (RMSE), pattern correlation coefficient (PCC), and Taylor skill score (TSS) (Wu et al. 2019). To evaluate the spatial distribution differences, the 3-hourly observational data were first averaged over time, and the resulting fields were then linearly interpolated to the model grid points to reconcile the spatial resolution mismatch. The statistical equations are provided below:

$$BIAS = \frac{1}{N}\sum_{i=1}^{N}(S_i - O_i) \tag{1}$$

$$\mathrm{RMSE} = \sqrt{\frac{1}{N}\sum_{i=1}^{N}(M_i - O_i)^2} \tag{2}$$

$$\mathrm{PCC} = \frac{\sum_{i=1}^{N}(M_i-\overline{M})(O_i-\overline{O})}{\sqrt{\sum_{i=1}^{N}(M_i-\overline{M})^2}\sqrt{\sum_{i=1}^{N}(O_i-\overline{O})^2}} \tag{3}$$

$$\mathrm{TSS} = \frac{4(1+PC)}{(\sigma+1/\sigma)^2(1+PC_0)} \tag{4}$$

In Eq. (4), σ is the standard deviation of the model values, normalized by that of the observations. The equation is as follows:

Table 1 Key characteristics and length variation of the studied glaciers on the TP (arranged in ascending order of longitude within each subregion), with data sourced from Yao et al. (2012b)

Subregions	Glacier ID	Glacier name	Latitude	Longitude	Area (km^2)	Length (km)	Orientation	Change (m yr^{-1})
1. West Himalayas	1	Samudra Tapu	32°30′	77°30′	73	17.7	E	−19.5
	2	Dunagiri	30°54′	78°51′	2.56	–	–	−3
	3	Satopanth	30°56′	78°53′	12	–	–	−26.9
	4	Milam	30°26′	80°03′	37	16.7	SE	−26.6
	5	Naimona'nyi	30°27′	81°20′	7.8	7.7	N	−5
2. Central Himalayas	6	Dasuopu	28°25′	85°41′	43.98	14.3	NE	−4.1
	7	Middle Rongbu	28°03′	85°50′	85.4	22.4	N/NW	−8.8
	8	AX010	27°42′	86°34′	0.38	1.7	E/SE	−6.9
	9	Qiangyong	28°51′	90°13′	7.98	5.5	N	−2.4
3. Southeast TP	10	Yanong	29°19′	96°42′	191	32.5	E/SE	−73
	11	Ata	29°10′	96°48′	13.8	16.7	S	−56.1
	12	Parlung No.4	29°14′	96°55′	11.7	8	N	−15.6
4. Western Nyainqentanglha	13	Gurenhekou	30°11′	90°27′	1.4	2.9	SE	−8.1
	14	Zhadang	30°29′	90°39′	2	2.5	NW	−10.8
5. Tanggula	15	Purogangri	33°57′	89°06′	18.5	9.1	SW	−1.7
	16	Malan	35°50′	90°47′	37.8	8.1	SE	−1
	17	Xiaodongkemadi	33°10′	92°08′	1.8	2.8	S/SW	−3.4
6. West Kunlun	18	Kunlun	35°26′	80°47′	200	23.6	NE	27.3
	19	Duofeng	35°25′	80°58′	251.7	31	NE	−27.6
	20	Yulong	35°24′	81°18′	139.07	30.9	NE/NW	16.3

$$\sigma = \sqrt{\frac{1}{N}\sum_{i=1}^{N}(M_i - \overline{M})^2} / \sqrt{\frac{1}{N}\sum_{i=1}^{N}(O_i - \overline{O})^2} \quad (5)$$

where N is the total number of data samples, which refers to either the number of time steps (for time series comparisons) or spatial grid points (for spatial distribution evaluations), depending on the context. $M_i(O_i)$ denotes the model (observed) value of sample i, $\overline{M}(\overline{O})$ represents the corresponding mean over the N samples. All evaluations were based on daily or seasonal averages derived from the original 3-hourly data.

3 Model evaluation

3.1 Lake surface water temperature

To evaluate the model's performance in simulating LSWT, we compared the simulated LSWT from WRF with in-situ observations (Li et al. 2016) and the C3S_LSWT satellite product for Qinghai Lake and Nam Co, the largest and third-largest lakes on the TP, respectively.

As shown in Fig. 2, the WRF-Lake model captured the seasonal evolution of LSWT in both large lakes. Both lakes reached their maximum LSWT in August during the open-water period and remained ice-covered from December/January to March/April during the cold season. Compared to the C3S_LSWT satellite product, the model simulated slightly higher LSWTs, with a BIAS of 0.72 °C and 0.90 °C, and an RMSE of 2.08 °C and 2.10 °C for Qinghai Lake and Nam Co, respectively. The largest differences occurred during the summer (JJA) months and gradually decreased toward winter (DJF), when the model values became slightly lower than satellite estimates. However, since satellite-derived LSWTs over the TP are typically 0.8–1.9 °C lower than in-situ measurements due to the cool-skin effect (Donlon et al. 2002; Ke and Song 2014), the actual model performance may be more accurate than the satellite comparison suggests. When evaluated against in-situ data at Qinghai Lake, the BIAS and RMSE improved to 0.52 °C and 0.87 °C, respectively.

The model also captures the observed subtle differences in the LSWT seasonal evolution between the two lakes: (a) the annual maximum LSWT of Qinghai Lake is 18.0 °C, significantly higher than that of Nam Co, which is 13.8 °C, mainly due to the lower elevation of Qinghai Lake; (b) Qinghai Lake warms faster in early summer (JJA) and also cools faster in autumn (SON) compared to Nam Co, primarily due to its shallower depth; and (c) the ice-on and ice-off dates of Qinghai Lake occur earlier than those for Nam Co, a result of the combined effects of its lower elevation and

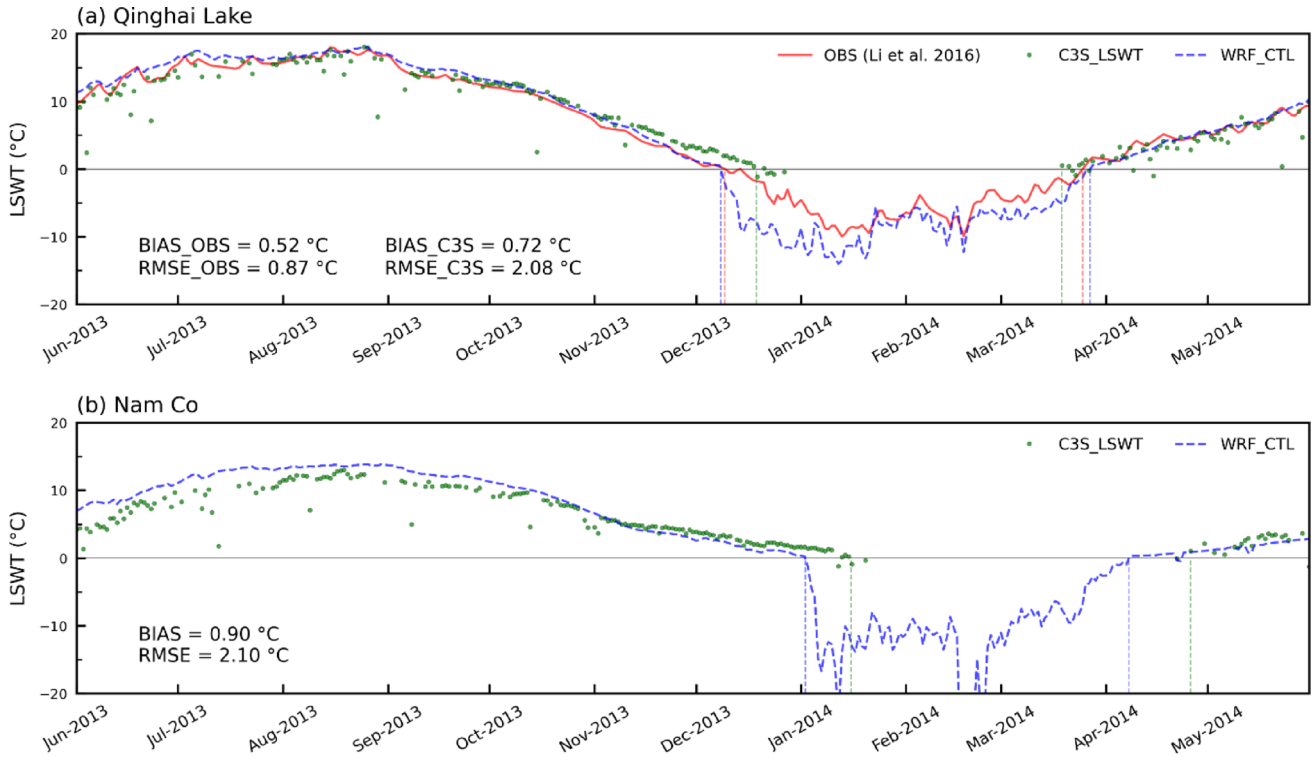

Fig. 2 The daily lake surface water temperature (LSWT) from in-situ observations (Li et al. 2016) for Qinghai Lake (red line), the C3S_LSWT product (green dots), and WRF_CTL simulations (blue dashed line) extracted from the central grid point of (a) Qinghai Lake and (b) Nam Co during the simulation period. Ice-on and ice-off dates are marked with vertical dashed lines in the same color as their corresponding LSWT data lines

shallower depth. In addition, differences in ice thickness may also contribute to the winter LSWT variation between the two lakes. These results indicate that the WRF model, with the lake scheme, provides a reasonable simulation of LSWT evolution and ice phenology for large lakes on the TP, making it suitable for studying the climatic effects of lakes on glaciers.

3.2 T_{2m} and precipitation

As shown in Fig. 3, cross-validation of ERA5-Land and WRF-simulated 2-m air temperature (T_{2m}), averaged over the entire study period, demonstrates that the model reliably captures the spatial distribution of T_{2m} across the TP. T_{2m} is strongly correlated with topography, generally decreasing with increasing altitude. Most regions, except for the northeastern, eastern, southeastern, and some southern areas of the TP, have an average T_{2m} below 0 °C, with the lowest values found in the Karakoram Mountains in the northwestern TP, where T_{2m} averages around −16 °C. Compared to ERA5-Land data, the WRF model simulates higher T_{2m} values in the eastern TP and lower values in the western TP, with deviations exceeding 2 °C in these areas. However, in most regions of the TP, the deviation is less than 2 °C, which is significantly less than the discrepancy found when comparing the model with MODIS observation (Meng et al. 2018). Performance metrics, including an RMSE of 1.8 °C, a PCC of 0.99, and a TSS of 0.97 (Table 2), calculated based on time-averaged T_{2m} fields, further confirm the relative accuracy of the model in simulating T_{2m}.

Comparison with IMERG observations indicates that the WRF model effectively reproduces the spatial pattern of precipitation, with most precipitation concentrated in low-elevation regions surrounding the TP, such as the southern slopes of the Himalayas, the Indian Peninsula, and the northern Bay of Bengal. In contrast, precipitation is lower over the TP, especially in the northwestern region. The primary discrepancies between simulation and observation are in precipitation magnitude: the WRF model overestimates precipitation over the Karakoram Mountains and underestimates it along the Himalayas, with an RMSE of 1.63 mm d^{-1}, a PCC of 0.78, and a TSS of 0.79. These metrics demonstrate the WRF model's strong capability to simulate precipitation patterns.

While the annual-mean evaluation confirms the model's overall reliability, seasonal validation remains essential to avoid compensating biases and to more accurately characterize the seasonal variability of lake-glacier interactions.

Figure 4 illustrates the seasonal differences in T_{2m} and precipitation between model simulations and observations. For T_{2m} (Fig. 4a–d), the smallest biases occur during summer (JJA), with slight overestimations primarily located west of the TP boundary and in scattered regions over the central-southern TP, generally within ± 5.3°C. In autumn (SON),

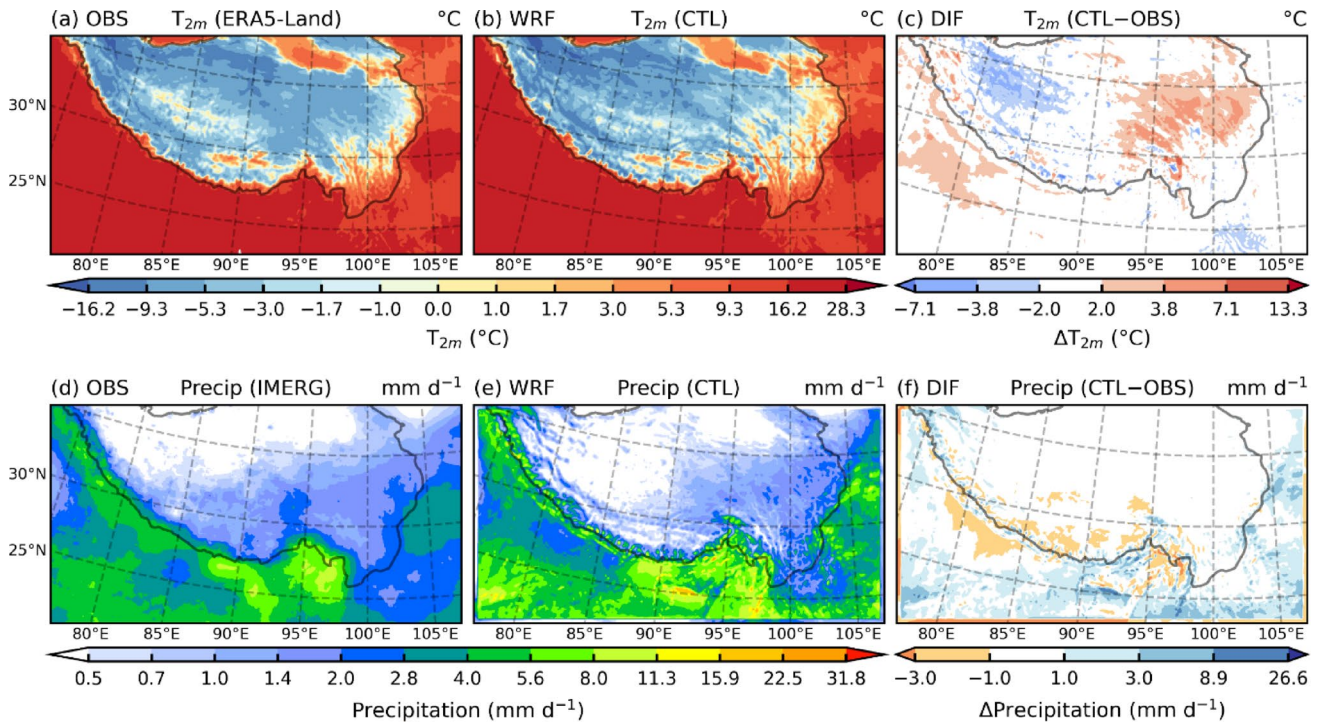

Fig. 3 Annual mean (**a**, **b**) 2-m air temperature (T_{2m}) and (**d**, **e**) precipitation from (**a**, **d**) observations and (**b**, **e**) CTL simulations, along with (**c**, **f**) their differences between CTL and observations, during the entire study period (June 2013–May 2014). The black contour indicates the 3000m elevation, outlining the TP

Table 2 Statistical comparison between WRF-simulated and observed 2-m air temperature (T_{2m}) and precipitation over Domain 2, based on annual (ANN) and seasonal means of summer (JJA), autumn (SON), winter (DJF), and spring (MAM) over the entire study period from June 2013 to May 2014. For each variable, 3-hourly data were first averaged in time to obtain annual and seasonal means, and then the spatial distributions of the variables were evaluated using the root-mean-square error (RMSE), pattern correlation coefficient (PCC), and Taylor skill score (TSS)

Variables	Metric	ANN	JJA	SON	DJF	MAM
T_{2m}	RMSE (°C)	1.80	1.70	1.96	2.59	2.34
	PCC	0.99	0.99	0.99	0.98	0.99
	TSS	0.97	0.99	0.99	0.99	0.99
Precipitation	RMSE (mm d^{-1})	1.63	4.21	1.57	0.84	1.59
	PCC	0.78	0.77	0.74	0.72	0.75
	TSS	0.79	0.78	0.79	0.66	0.70

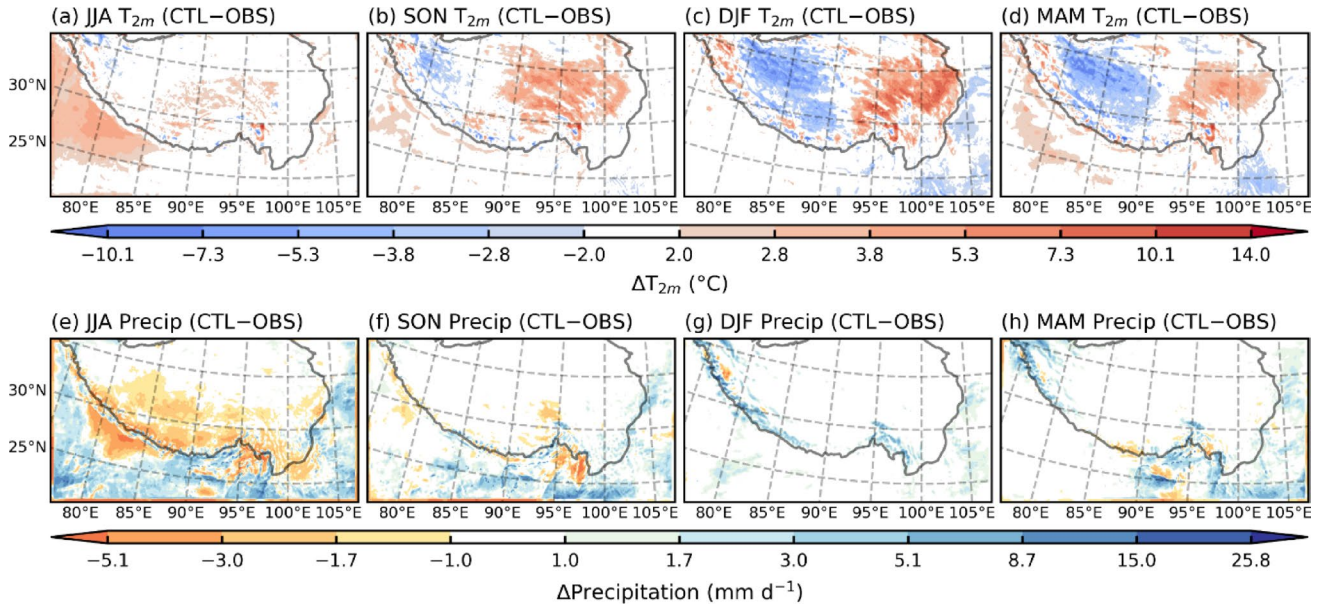

Fig. 4 Seasonal mean differences between WRF-simulated and observed (**a**–**d**) T_{2m} and (**e**–**h**) precipitation over Domain 2 during the entire study period (June 2013–May 2014). Panels correspond to (**a**, **e**) summer (JJA), (**b**, **f**) autumn (SON), (**c**, **g**) winter (DJF), and (**d**, **h**) spring (MAM), respectively. The black contour indicates the 3000 m elevation, outlining the TP

the spatial bias pattern resembles the annual mean, exhibiting cold biases in the western TP (mostly within − 7.3°C) and warm biases in the eastern TP (within + 7.3°C). This east–west contrast intensifies in winter (DJF), where biases range from − 10.1°C to + 10.1°C, while spring (MAM) shows a similar but less pronounced distribution (− 10.1°C to + 7.3°C). Across all seasons, PCCs remain high (≥ 0.98), with RMSE values ranging from 1.70°C in summer to 2.59°C in winter, and TSSs consistently above 0.99 (Table 2), demonstrating the model's robust skill in capturing seasonal T_{2m} variations.

Regarding precipitation (Fig. 4e–h), biases exhibit notable spatial heterogeneity. During summer, the model significantly underestimates precipitation along the southern and northern flanks of the Himalayas, mirroring the spatial pattern of the annual mean but with greater magnitude—maximum deviations reach up to − 5.1 mm d^{-1}. In autumn, precipitation biases are generally minor across most of the TP, remaining within ± 1 mm d^{-1}; however, a distinct underestimation occurs in the southeastern TP, with biases reaching up to − 3.0 mm d^{-1}. In winter and spring, precipitation is overestimated over the West Himalayas, Karakoram, and southeastern TP ranges, with maximum positive biases not exceeding 8.7 mm d^{-1}, while most other regions exhibit relatively minor biases within ± 1 mm d^{-1}. Seasonal RMSE values range from 0.84 mm d^{-1} in winter to 4.21 mm d^{-1} in summer, and both PCCs (0.72–0.77) and TSSs (0.66–0.79) remain relatively stable across seasons (Table 2), confirming the model's capability to reproduce seasonal precipitation patterns reliably.

Overall, these results indicate that despite strong agreement in annual metrics, some seasonal discrepancies persist—particularly in winter temperature and summer precipitation biases. Nonetheless, these deviations are within acceptable ranges, emphasizing the importance of seasonal-scale validation for accurately assessing lake-induced influences on glacier dynamics.

4 Seasonal climatic effects of TP lakes: spatial distribution and on different glaciers

4.1 Lake effects on surface air temperature T_{2m}

Glaciers are highly sensitive to changes in T_{2m} (Rounce et al. 2023). To examine the seasonal effects of TP lakes on glaciers, this study first analyzed lake-induced variations in T_{2m} by comparing the CTL and SEN experiments. As shown in Fig. 5, the spatial distribution of T_{2m} differences between the CTL and SEN experiments varies significantly by season. In our simulations, TP lakes generally show a cooling tendency in summer over lake surfaces and nearby land (Fig. 5a). T_{2m} decreased by approximately −0.1 °C to −1.4 °C across the southern and most of the eastern Inner TP due to the presence of lakes, except for a small area where T_{2m} slightly increased by about 0.1 °C to 0.4 °C. Consequently, many alpine glaciers in these regions, such as those in the western Nyainqentanglha Range (Subregion 4) and Tanggula Mountains (Subregion 5), experienced a decrease in T_{2m}, which could contribute to reduced ablation under the simulated conditions. In autumn, the lake effect on T_{2m} becomes more complex (Fig. 5b). Although most TP lakes act as substantial heat and moisture sources, raising T_{2m} over lake surfaces by 0.1 °C to 2.6 °C, T_{2m} over surrounding land decreases significantly by −0.1 °C to −5.1 °C. This lake-induced cooling supports the preservation of alpine glaciers around those lakes in subregions 2, 4, and 5. The winter pattern of lake-induced T_{2m} changes is similar to autumn, except weakened warming effect over lake surfaces due to ice cover, with T_{2m} increasing by only 0.1°C to 1.4°C over lakes, while surrounding land experiences a substantial cooling of −0.1°C to −5.1°C, further aiding glacier preservation in subregions 2, 4, and 5 (Fig. 5c). In spring, as lake ice melts, small and medium-sized lakes in the southern Inner TP exert a slight warming effect over lakes, increasing T_{2m} over lake surfaces by about 0.1 °C to 0.7 °C. However, T_{2m} over adjacent land decreases by −0.1 °C to −5.1 °C, continuing to promote glacier preservation in subregions 4 and 5 (Fig. 5d).

Overall, TP lakes tend to decrease T_{2m} over the surrounding land in many seasons in our experiments, including

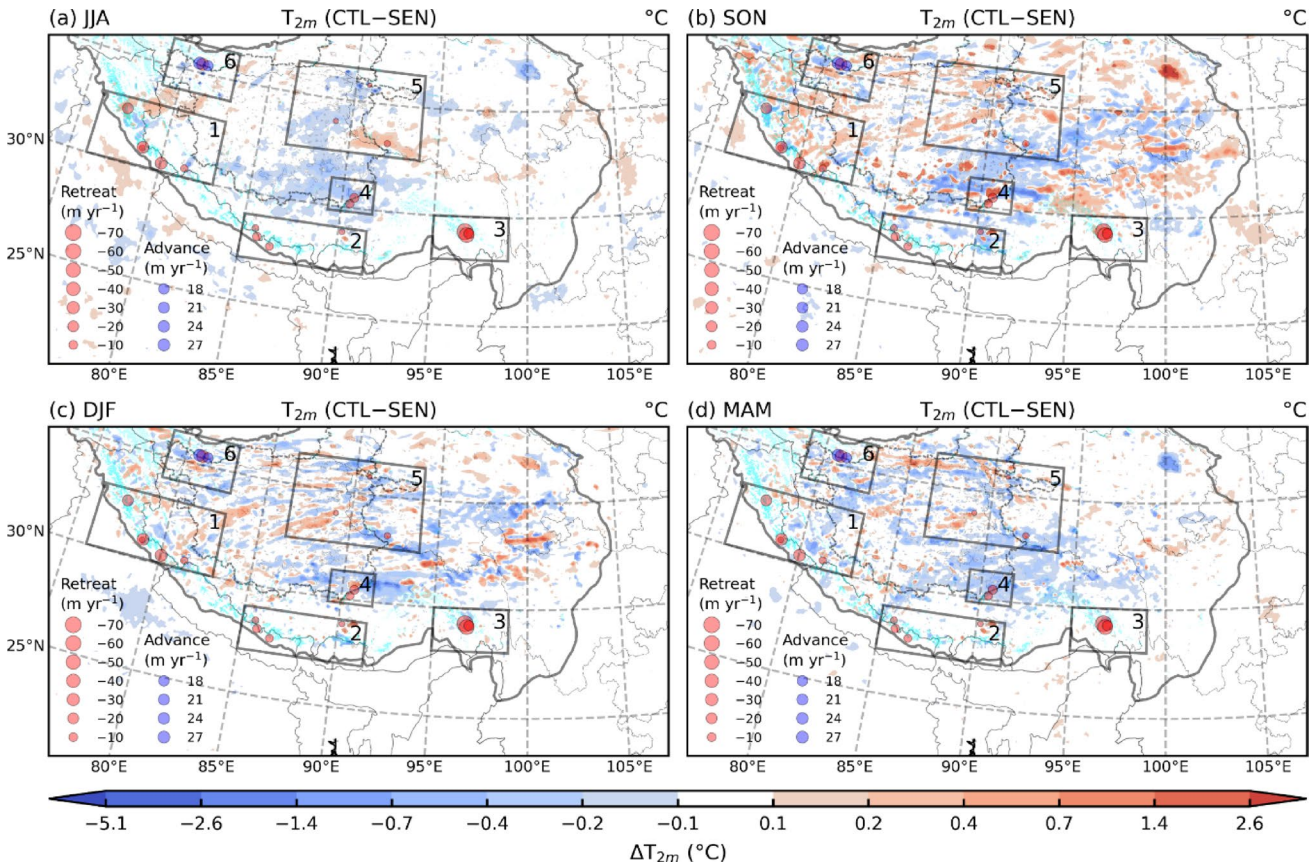

Fig. 5 The mean differences in simulated T_{2m} between the CTL and SEN experiments during **a** summer (JJA), **b** autumn (SON), **c** winter (DJF), and **d** spring (MAM). The black boxes indicate subregions 1–6. The solid black line represents the 3000 m elevation contour outlining the TP, while the dashed line outlines the Inner TP. The cyan areas represent glacier distribution, and the red (retreating) and blue (advancing) filled circles correspond to glaciers listed in Table 1, with circle sizes indicating glacier change rates over recent decades (Yao et al. 2012b)

autumn in certain areas, despite the warming simulated directly over lake surfaces. The cooling effect of TP lakes is most pronounced in summer and over the southern and eastern Inner TP, where lake density is highest. Consequently, glaciers in Subregions 4 and 5 experience a lake-induced decrease in T_{2m}, which helps to mitigate glacier retreat.

Figure 6 provides a detailed analysis of lake-induced seasonal changes in daily maximum 2-m air temperature (T_{2m_Dmax}) over all 20 glaciers in each subregion listed in Table 1, as well as T_{2m_Dmax} from the CTL experiment.

In summer, TP lakes primarily induce a cooling effect, lowering T_{2m_Dmax} over most glaciers. Notable decreases include the Dasuopu Glacier (−0.15 °C) and Qiangyong Glacier (−0.20 °C) in the Central Himalayas, the Gurenhekou Glacier (−0.28 °C) and Zhadang Glacier (−0.17 °C) in the Nyainqentanglha Mountains. An exception is the Xiaodongkemadi Glacier in the Tanggula Mountains, where T_{2m_Dmax} increased by approximately 0.20 °C. Since T_{2m_Dmax} generally exceeds the freezing point over these glaciers in summer, the lake-induced cooling may slightly mitigate glacier retreat, particularly for glaciers like Dasuopu, where T_{2m_Dmax} is near the freezing point. However, in the West Kunlun Mountains, the impact of lake-induced T_{2m_Dmax} changes on glaciers is limited due to both the small warming magnitude and the persistently sub-freezing baseline temperatures, which together restrict the potential for glacier melting in this region. In autumn, simulated cooling near lakes such as Langa Co and Mapam Yumco produces

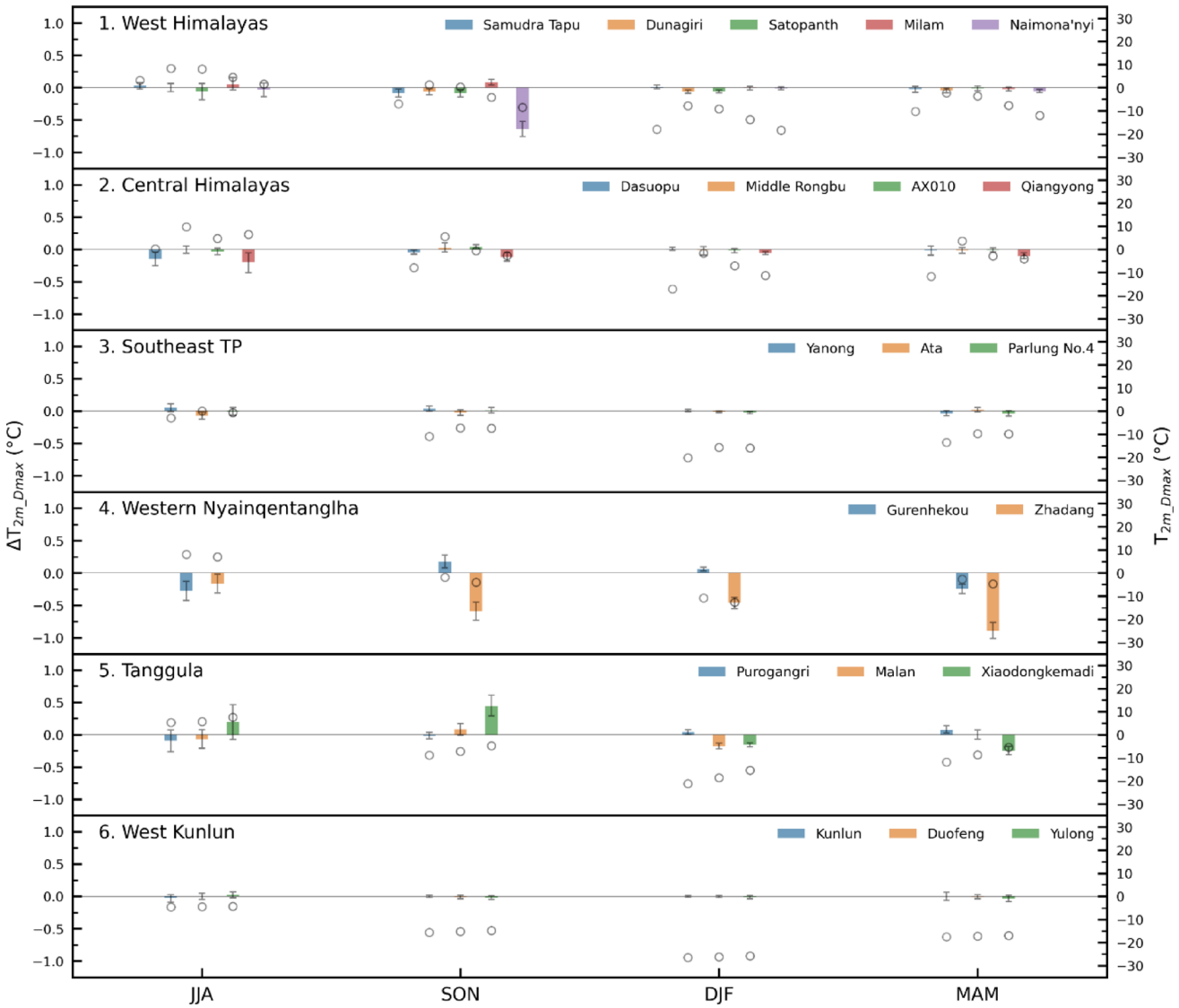

Fig. 6 Lake-induced changes in daily maximum 2-m air temperatures (T_{2m_Dmax}) averaged over summer (JJA), autumn (SON), winter (DJF), and spring (MAM) for glacier grids within each subregion depicted in Fig. 5 (bars, ordered by longitude from left to right). The black hollow circles indicate the seasonally averaged T_{2m_Dmax} on the corresponding glacier grid as simulated by the CTL experiment. Error bars represent the 95% confidence interval estimated via bootstrap resampling

a relatively large T_{2m_Dmax} decrease (−0.64 °C) at the Naimona'nyi Glacier in our simulation. This localized cooling is consistent with observed slower retreat rates. For glaciers in the western Nyainqentanglha Range (Subregion 4), lake effects differ by slope: Gurenhekou Glacier shows a T_{2m_Dmax} increase of 0.18 °C, while Zhadang Glacier experiences a further decrease of −0.59 °C, indicating differing climatic impacts from Nam Co on glaciers on the south versus north slopes. In the Tanggula Mountains, Xiaodongkemadi Glacier shows a significant T_{2m_Dmax} increase of 0.44°C, critical given its T_{2m_Dmax} is only −4.83°C, contributing to its rapid retreat compared to other glaciers in the range. In winter, Zhadang Glacier on the north slope of the western Nyainqentanglha Range (subregion 4) experiences the largest change in T_{2m_Dmax} (−0.46°C), whereas T_{2m_Dmax} change at Gurenhekou Glacier on the south slope is reduced to negligible levels. The Malan and Xiaodongkemadi glaciers in the Tanggula Mountains (subregion 5) experience minor decreases in T_{2m_Dmax} of −0.18°C and −0.16°C, respectively. In spring, Nam Co induces a pronounced cooling effect, reducing T_{2m_Dmax} by −0.89°C at Zhadang Glacier and −0.24°C at Gurenhekou Glacier. Such cooling plays a critical role in glacier preservation, as it ensures that T_{2m_Dmax} remains well below the melting point, with respective values of −4.64°C and −2.67°C.

Overall, the simulations indicate that TP lakes can influence glacier thermal conditions, with cooling signals prevailing in many regions and seasons in our experiments. In summer, the cooling effect mitigates glacier retreat, especially for those with T_{2m_Dmax} near the freezing point, while exceptions like Xiaodongkemadi Glacier experience warming. Autumn sees intensified cooling in areas like the West Himalayas, slowing glacier retreat. The impacts of TP lakes in winter and spring vary by location, with Nam Co providing springtime cooling for glacier preservation. These effects suggest a complex and region-specific role of TP lakes in shaping glacier dynamics.

4.2 Lake effects on snowfall

Figure 7 shows seasonal snowfall differences between the CTL and SEN experiments. Even in summer (Fig. 7a), the simulations produce measurable lake-related snowfall changes in some high-altitude areas. Across most glacier-covered areas, TP lakes generally increase snowfall, except in the northern parts of Subregion 1 and the southern parts of Subregion 5, where snowfall may be reduced due to the influence of TP lakes. Lake-induced snowfall changes are most pronounced in autumn (Fig. 7b), likely due to the strong lake effect during this season, which is also confirmed by previous studies (Zhao et al. 2022b; Zhu et al. 2020). The distribution of snowfall changes aligns with glacier locations, revealing that TP lakes enhance snowfall over most glaciers, with only a few glaciers in the Southeast TP (Subregion 3) experiencing reduced snowfall. In winter (Fig. 7c), despite the typically snowy conditions, lake-induced changes in snowfall are minimal across the Inner TP, likely due to ice cover formation over lakes, which weakens their climatic influence. However, compared to summer and autumn, lake-induced snowfall increases are more significant in winter over glaciers in the West Himalayas (Subregion 1). In spring (Fig. 7d), as in winter, most TP lakes remain frozen, resulting in minimal lake-induced snowfall changes in the Inner TP. Nonetheless, model results suggest a possible increase in spring snowfall over the West Himalayas (Subregion 1), which may be partly related to the lake effect.

To further quantify the impact of lake-induced snowfall changes on glacier behavior, seasonal average changes in daily snowfall over glaciers in each subregion were examined (Fig. 8).

In summer, snowfall was generally minimal over most glaciers, except for those in the Southeast TP (Subregion 3), such as Yanong Glacier, Ata Glacier, and Parlung No. 4 Glacier, where snowfall was significantly enhanced by the Indian Summer Monsoon (Shaw et al. 2022). The lake-induced snowfall changes on these glaciers were simulated at −0.11 mm d^{-1} (−2.8%), 0.20 mm d^{-1} (11.5%), and 0.09 mm d^{-1} (5.1%), respectively. In the West and Central Himalayas, glaciers adjacent to lakes tend to experience greater snowfall increase and slower retreat, including Naimona'nyi Glacier, near Langa Co and Mapam Yumco, with a rise of 0.08 mm d^{-1} (6.6%); Dasuopu Glacier, adjacent to Paiku Co, with 0.18 mm d^{-1} (12.2%); and Qiangyong Glacier, near Yamzho Yumco and Puma Yumco, with 0.06 mm d^{-1} (55.2%). In the western Nyainqentanglha Range (Subregion 4), Nam Co exerted distinct climatic impacts on its south and north slopes, with snowfall increasing by 0.05 mm d^{-1} (38.1%) over Gurenhekou Glacier while decreasing by −0.09 mm d^{-1} (−40.2%) over Zhadang Glacier.

In autumn, lake-induced snowfall generally increased on glaciers in the West Himalayas (Subregion 1), with the most pronounced change of 0.17 mm d^{-1} (26.4%) observed on Naimona'nyi Glacier, attributed to the intensified climatic effect of Langa Co and Mapam Yumco. In the Central Himalayas (Subregion 2), only Qiangyong Glacier experienced a modest increase in snowfall of 0.04 mm d^{-1} (8.1%) due to nearby lakes. For Gurenhekou and Zhadang glaciers in the western Nyainqentanglha Range (Subregion 4), Nam Co generally decreases snowfall over these glaciers, with a notable reduction of −0.16 mm d^{-1} (−28.0%) over Gurenhekou Glacier. In the West Kunlun Mountains (Subregion 6), Yulong Glacier experienced the most significant increase in snowfall of 0.11 mm d^{-1} (21.1%).

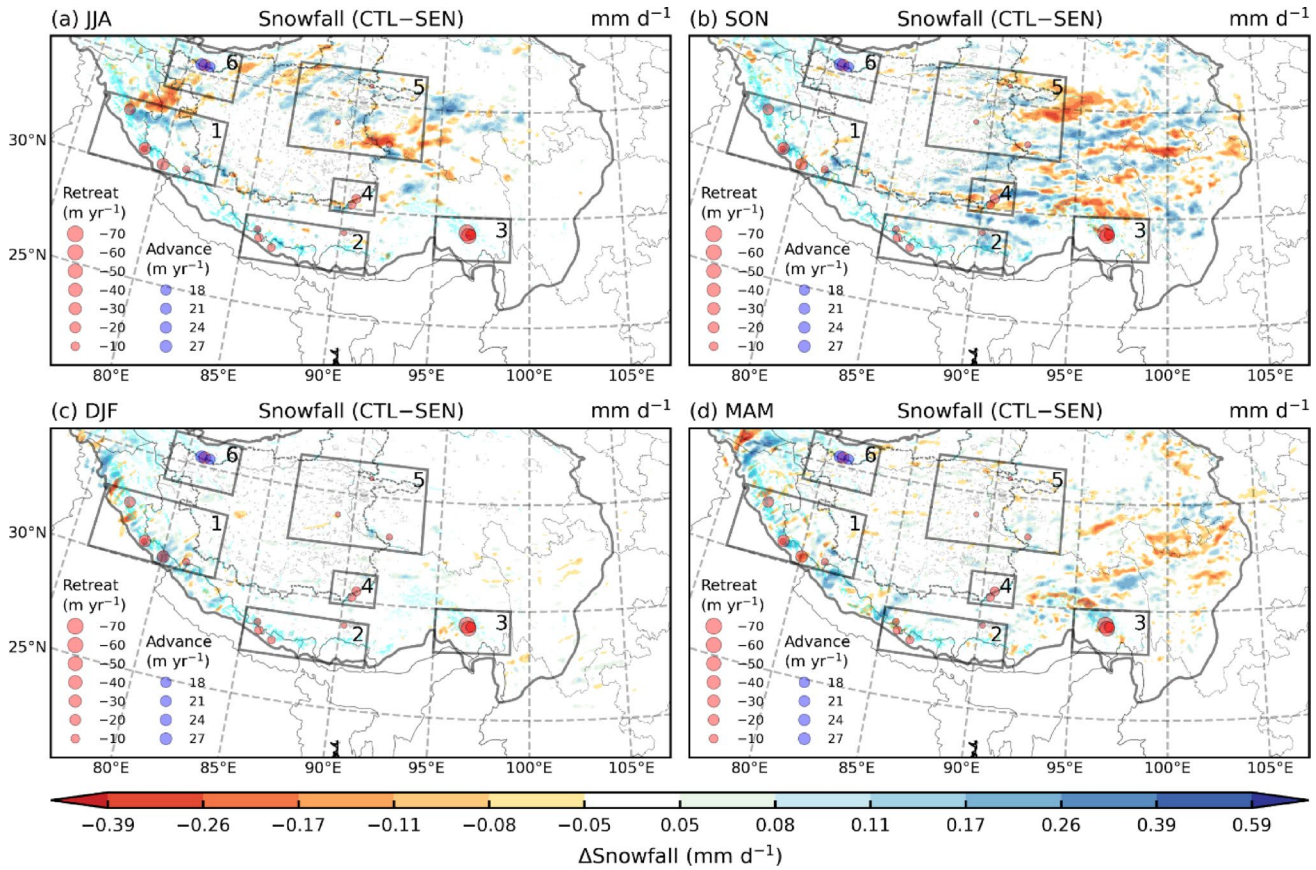

Fig. 7 Same as Fig. 5, but for snowfall

In winter, lake-induced changes in snowfall on glaciers were generally reduced, except for Milam Glacier and Dasuopu Glacier in the West and Central Himalayas (Subregions 1 and 2), which experienced significant snowfall increases of 0.18 mm d^{-1} and 0.10 mm d^{-1}, respectively. However, since snowfall also increased significantly, particularly in the West and Central Himalayas (Subregions 1 and 2), the contribution of lake-induced snowfall to the total snowfall on these two glaciers was relatively minor, at only 4.7% and 2.5%, respectively. In contrast, for Zhadang Glacier in the western Nyainqentanglha Range and Xiaodongkemadi Glacier in the Tanggula Mountains, the lake-induced snowfall contributed the most, at 55.1% and 16.0%, respectively, despite their small changes in magnitude of less than 0.1 mm d^{-1}.

In spring, the TP lakes have negligible impacts on snowfall for most glaciers, except for Milam Glacier in the West Himalayas (Subregion 1), and Dasuopu and Qiangyong Glaciers in the Central Himalayas (Subregion 2), which experienced significant changes in snowfall of −0.27 mm d^{-1} (−8.1%), −0.12 mm d^{-1} (−8.7%), and 0.10 mm d^{-1} (38.7%), respectively. In contrast, Gurenhekou and Zhadang Glaciers in the western Nyainqentanglha Range experienced a modest but significant contribution of lake-induced snowfall, with increases of 0.03 mm d^{-1} (47.2%) and 0.07 mm d^{-1} (43.5%), respectively.

Overall, in our simulations, TP lakes appear to be important contributors to local snowfall variability on some glaciers, particularly in summer and autumn when lake-atmosphere interactions tend to be strongest. In the model results, glaciers adjacent to lakes generally show larger lake-related snowfall anomalies than those farther away. Therefore, the following sections will focus on investigating the climatic effects of lakes on adjacent glaciers during summer and autumn.

4.3 Effects of specific lakes on adjacent glaciers

4.3.1 West Himalayas (Subregion 1): Langa Co and Mapam Yumco

Figure 9 illustrates the effects of lake-induced changes in T_{2m} and snowfall on glaciers surrounding Langa Co (4,575 m a.s.l., 49 m depth) and Mapam Yumco (4588 m a.s.l., 70 m depth). During summer (Fig. 9a), both lakes—particularly Mapam Yumco—induced a cooling effect, reducing T_{2m} by 0.1 °C to 0.7 °C over the lake surfaces, with a decrease of 0.1 °C to 0.4 °C in the surrounding areas. While

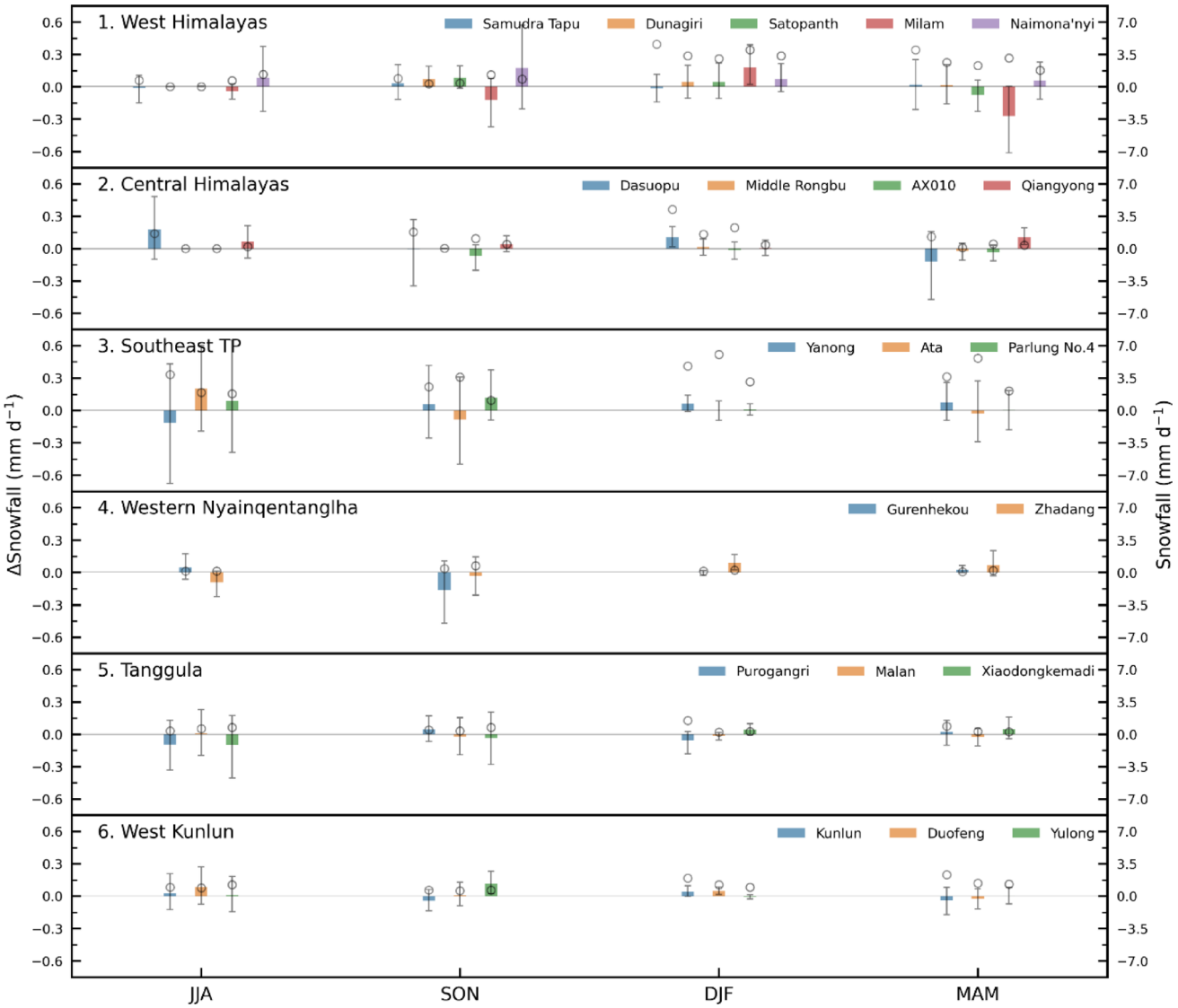

Fig. 8 Same as Fig. 6, but showing lake-induced changes in daily snowfall averaged over summer (JJA), autumn (SON), winter (DJF), and spring (MAM)

the cooling effect was prominent over the lake surfaces, the impact on the nearby glaciers was minimal. Only glaciers to the south and north of the lakes experienced slight decreases in T_{2m} (ranging from −0.1 °C to −0.2 °C), while glaciers to the southwest remained almost unaffected. In contrast, during autumn (Fig. 9b), both lakes contributed to a warming effect, with T_{2m} increasing by 0.4 °C to 0.7 °C over the lakes. This warming extended to the surrounding areas, particularly the southwest, where some glaciers experienced a T_{2m} increase ranging from 0.1 °C to 0.7 °C. However, glaciers south of the lakes showed significant cooling, with T_{2m} decreases ranging from −0.1 °C to −0.7 °C, particularly on the summit region of Naimona'nyi Glacier (marked by red-filled circles south of the lakes), where T_{2m} decreased by −0.7 °C to −2.5 °C.

Langa Co and Mapam Yumco also significantly influenced snowfall around the surrounding glaciers. In summer (Fig. 9a, c), convergence between northerly lake breezes (blowing southward from Langa Co and Mapam Yumco) and large-scale southerly winds (blowing northward) over the glacier regions enhanced snowfall, particularly over areas with elevations above 5200 m and average T_{2m} below 5 °C. However, glaciers to the southwest and northeast of the lakes experienced reduced snowfall, with decreases ranging from −0.05 mm d^{-1} to −0.17 mm d^{-1}. In autumn (Fig. 9b, d), the lakes' warming effect created updrafts and converging flows, in addition to contrasting water-land surface friction, leading to divergence on the windward side and convergence on the leeward side (Yao et al. 2021). As a result, snowfall was reduced on the windward sides,

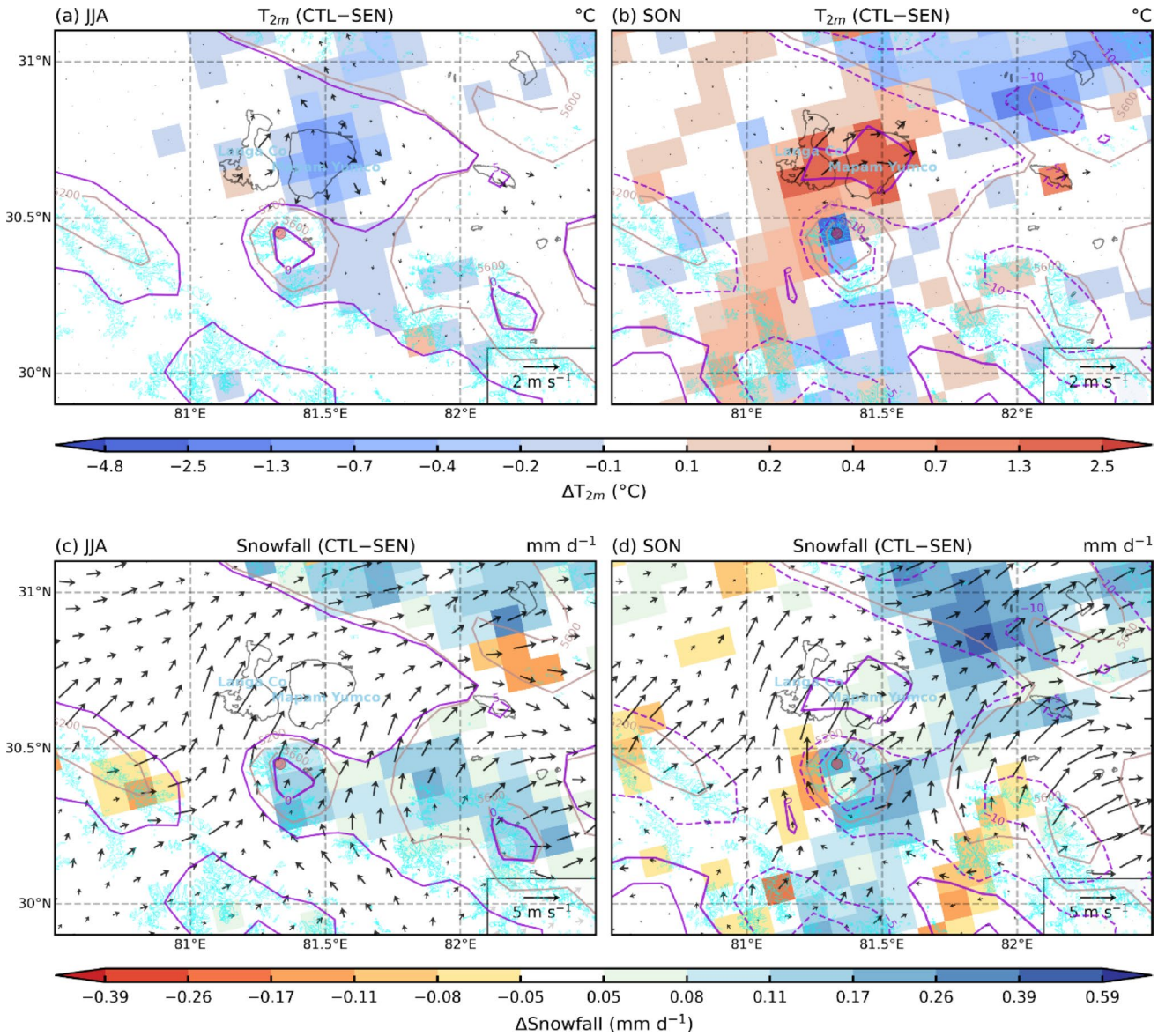

Fig. 9 The mean differences in simulated (a, b) T_{2m} and (c, d) snowfall between the CTL and SEN experiments during (a, c) summer (JJA) and (b, d) autumn (SON) around Langa Co and Mapam Yumco in the West Himalayas (Subregion 1). Arrows in (a, b) show 10 m wind differences (CTL − SEN), and those in (c, d) show 10 m wind fields from the CTL simulation. The brown contours represent terrain elevation, showing only altitudes above 5200 m. Purple contours denote the 0 °C isotherms (solid for ≥ 0 °C, dashed for < 0 °C). Cyan areas show glacier distributions, and a red-filled circle marks the location of the Naimona'nyi Glacier

negatively affecting the western portion of Naimona'nyi Glacier. On the south and leeward sides of the lakes, however, snowfall increased by approximately 0.05 mm d^{-1} to 0.59 mm d^{-1}, contributing to the preservation of glaciers such as the eastern Naimona'nyi Glacier (south of the lake) and glaciers to the north.

Generally, simulations suggest Langa Co and Mapam Yumco can notably modify local T_{2m} and snowfall near glaciers. In summer, they induce cooling with minimal glacier impact, while in autumn, they warm most areas but cool southern glaciers like Naimona'nyi Glacier (−2.5°C). Snowfall increases on northern and southern glaciers in summer but shifts to the leeward sides in autumn, benefiting glaciers like eastern Naimona'nyi. These simulated effects point to a potential role of individual lakes in modulating regional glacier-climate interactions.

4.3.2 Central Himalayas (Subregion 2): Yamzho Yumco and Puma Yumco

Figure 10 illustrates the localized climatic effects of Yamzho Yumco (4,400 m a.s.l., 19.06 m depth) and Puma Yumco

(5,030 m a.s.l., 47 m depth) on nearby glaciers during summer (JJA) and autumn (SON). In summer (Fig. 10a), Yamzho Yumco exerted a slight cooling effect, lowering T_{2m} over the lake by −0.1 °C to −0.4 °C. Conversely, Puma Yumco caused a warming effect, increasing T_{2m} over the lake by 0.1 °C to 0.7 °C. The difference in climate effect between these two lakes, as well as other lakes on the TP, is primarily attributed to their variations in altitude. Lakes at higher altitudes receive intensified solar radiation and concurrently experience lower air temperatures (T_{2m}), resulting in a positive lake-air temperature difference even during summer. As a result, the climatic impact of these lakes on nearby glaciers was generally minimal, with only the glaciers to the west of Yamzho Yumco showing a noticeable effect, experiencing a T_{2m} decrease ranging from −0.1 °C to −0.2 °C. In autumn (Fig. 10b), both lakes had a warming influence over their surface, particularly Yamzho Yumco, where T_{2m} increased by 0.1 °C to 2.5 °C. However, on surrounding land areas, both lakes contributed to a T_{2m} reduction of −0.1 °C to −2.5 °C, with a significant T_{2m} drop simulated over the glaciers around both lakes, including the Qiangyong Glacier to the west of Yamzho Yumco.

The impact of lake-induced changes in snowfall on the surrounding glaciers was also analyzed. During summer (Fig. 10c), the influence of both lakes on snowfall was minimal, with a marginal increase in snowfall of 0.05 mm d^{-1} to 0.11 mm d^{-1} on glaciers adjacent to the west of Yamzho Yumco and an increase of less than 0.17 mm d^{-1} on glaciers adjacent to the south of Puma Yumco. In autumn (Fig. 10d), both lakes contributed significantly to increased snowfall, particularly to glaciers south of Puma Yumco, where snowfall increased by 0.59 mm d^{-1}. Glaciers to the west

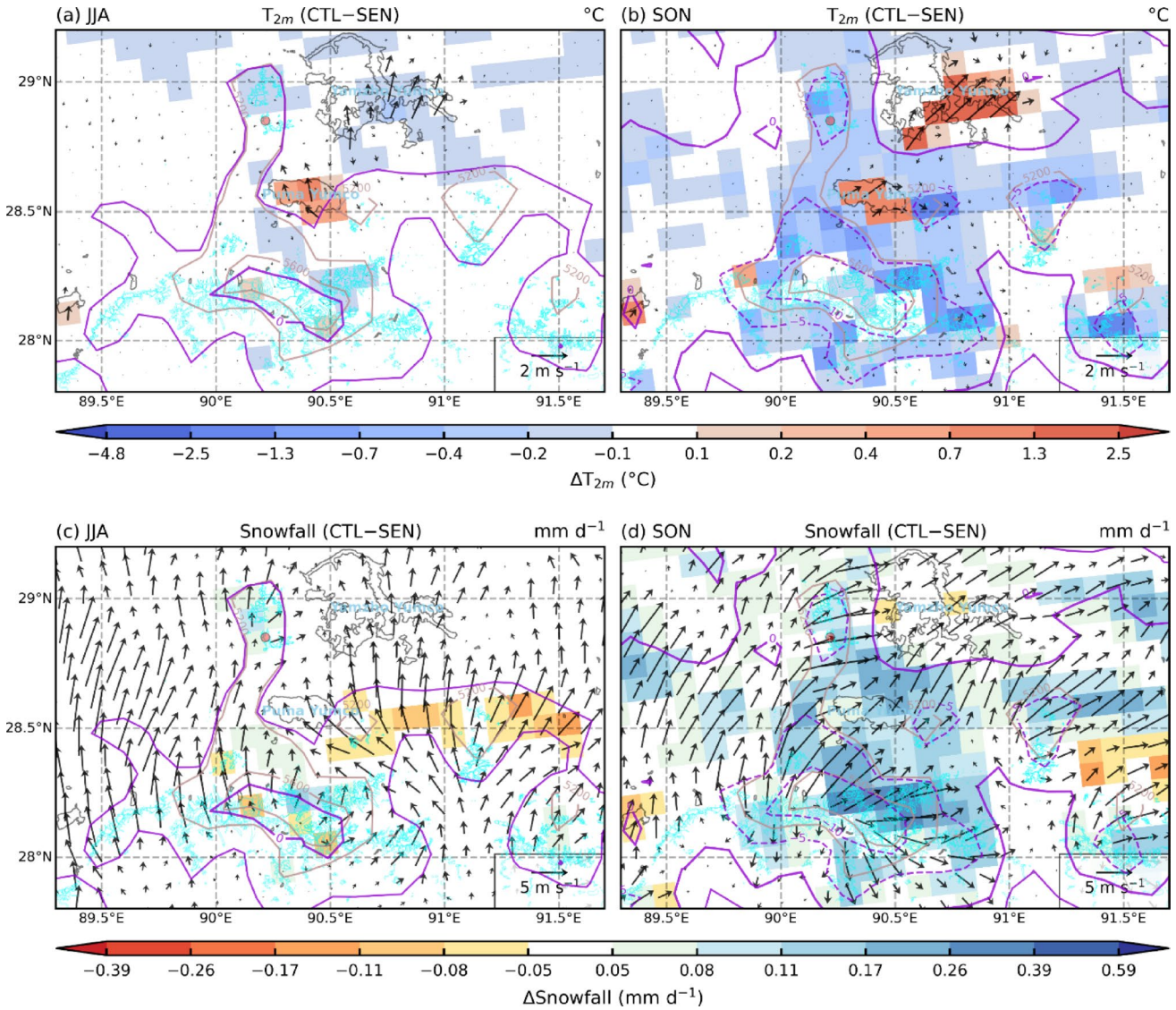

Fig. 10 Same as Fig. 9 but for the Yamzho Yumco and Puma Yumco region in the Central Himalayas (Subregion 2). The red-filled circle marks the location of the Qiangyong Glacier

of Yamzho Yumco, including the Qiangyong Glacier, also experience increases in snowfall, ranging from 0.05 mm d^{-1} to 0.17 mm d^{-1}.

Overall, in our simulations, Yamzho Yumco and Puma Yumco are associated with decreased T_{2m} and increased snowfall around some neighboring glaciers, with stronger signals in autumn in these experiments. The cooling effect on T_{2m} and the enhanced snowfall were especially evident around the glaciers west of Yamzho Yumco and south of Puma Yumco, suggesting more pronounced lake-induced climate effects during the colder autumn.

4.3.3 Western Nyainqentanglha (Subregion 4): Nam Co

Figure 11 illustrates the climatic impact of Nam Co, the second-largest lake in the Inner TP, on the glaciers in the western Nyainqentanglha Range. Situated on the north slope of the range, Nam Co exerts relatively large simulated perturbations on the local climate in our experiments. For example, it produces simulated summer cooling of up to ~ 1.3 °C in parts of the basin in this run. The glaciers in the western Nyainqentanglha Range experienced a decrease in T_{2m} of up to 0.7 °C. In autumn, the strong warming effect of Nam Co significantly increased T_{2m} over the lake surface by up to 2.5 °C. However, both western and eastern areas surrounding the lake experienced notable T_{2m} decreases, with the most pronounced cooling (up to 4.8 °C) occurring to the east. The glacier located east of the lake benefited from a T_{2m} reduction of up to 0.7 °C. For glaciers on the northern slope of the western Nyainqentanglha Range, adjacent to the southern shore of Nam Co—including Zhadang Glacier—T_{2m} decreased by approximately 0.1 °C to 0.4 °C. In contrast, on the southern slope, T_{2m} increased by about 0.1 °C to 0.7 °C.

In terms of snowfall distribution, Nam Co also plays a prominent role (Fig. 11c, d). In summer, the cooling effect of the lake leads to divergent winds over its southern shore, resulting in a reduction in snowfall on the northern slope of the western Nyainqentanglha Range by up to − 0.39 mm d^{-1}, while slightly enhancing snowfall on the southern slope by up to 0.17 mm d^{-1}. Conversely, Nam Co strengthens the west winds in autumn, which induce convergent airflow on the lake's leeward side, leading to increased snowfall. This simulated pattern is relatively pronounced for some glaciers east of the lake, where modeled snowfall increases reach up to ~ 0.59 mm d^{-1} in these experiments. However, glaciers situated south of Nam Co experienced a significant decrease in snowfall, with a reduction reaching as high as − 2.6 mm d^{-1}.

4.4 Lake effects on moisture transport

Evaporation from oceans serves as a critical source of moisture for glaciers in the TP (Li et al. 2022). To better understand how TP lakes influence glacier behavior through their impact on moisture transport, we analyzed the differences in vapor flux and vapor flux divergence between the CTL and SEN experiments.

During summer (Fig. 12a), in our experiments, TP lakes contribute to modifications of regional circulation that are associated with enhanced northward water vapor flux from the Indian Ocean and Bay of Bengal. The enhancement of vapor flux from the Indian Ocean and Bay of Bengal to the TP in the CTL experiment is not a direct result of lake evaporation outside the TP, but rather stems from lake-induced modifications in regional thermal and dynamical conditions. These include altered land–atmosphere energy exchanges and changes in surface pressure gradients, which in turn modulate the large-scale atmospheric circulation and monsoonal flow pathways. Such thermally induced circulation adjustments, particularly over the southern margin of the TP, facilitate the convergence and redirection of moist air masses into the interior TP. This moisture is transported into the TP through valleys in the Central and Eastern Himalayas (in Subregions 2 and 3). The external water vapor converges with vapor evaporated from lakes in the southern Inner TP, which is then transported clockwise along the Inner TP margins. In the simulations, this combined vapor flux is transported toward glaciers in parts of the western and northern TP, including the West Kunlun (Subregion 6) and Tanggula Mountains (Subregion 5), in some cases. The vapor flux divergence around most TP glaciers shows significant changes, particularly for glaciers in the western Nyainqentanglha Range (Subregion 4) and Tanggula Mountains (Subregion 5), which experience distinct water vapor convergence. In autumn, as westerly winds become dominant, TP lakes enhance the eastward vapor flux, especially over the southern TP. Compared to summer, only one main pathway for lake-induced external water vapor transport remains, flowing from southern Nepal through valleys in the Central Himalayas (Subregion 2). As a result, more water vapor is transported from Nepal and lakes in the southern Inner TP to the eastern TP. In this period, glaciers east of Subregion 2 experienced water vapor convergence, while the western Nyainqentanglha Range (Subregion 4) saw significant water vapor divergence. In winter, TP lakes slightly increase eastward flux over the southern Inner TP, exerting negligible influence on glaciers. In spring, TP lakes induce a similar vapor flux pattern as in winter, but with greater intensity, leading to significant vapor flux convergence on glaciers in the western Nyainqentanglha Range.

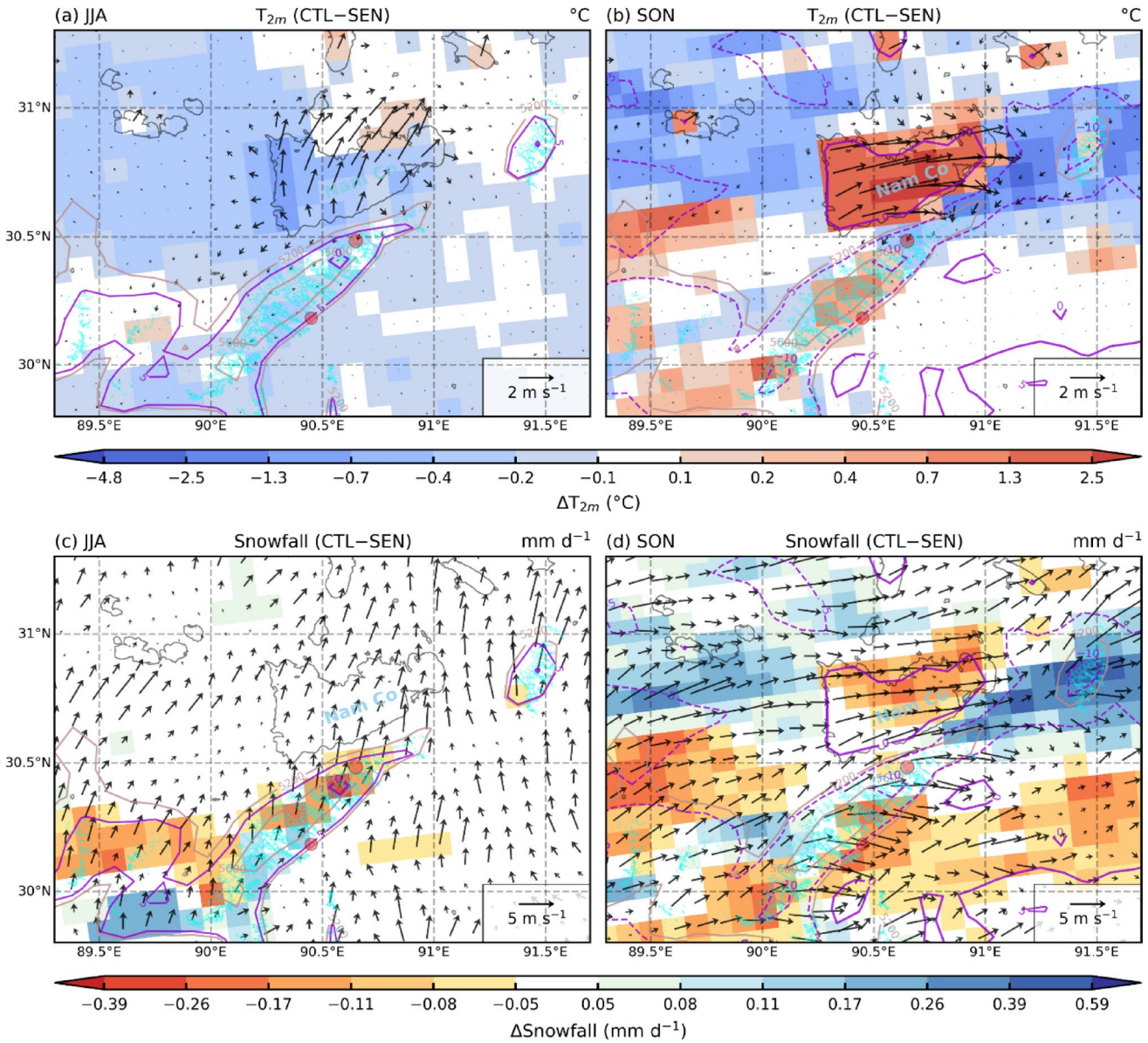

Fig. 11 Same as Fig. 9 but for the Nam Co region in the western Nyainqentanglha Range (Subregion 4). The red-filled circles indicate the Gurenhekou and Zhadang Glaciers

5 Discussion

To elucidate the mechanisms driving the spatial and seasonal variability of glacier responses, we examined how TP lakes influence local climatic conditions and glacier mass balance. Our simulations indicate that the climatic influence of TP lakes on glacier-relevant variables exhibits spatial heterogeneity and seasonal complexity, and that this simulated variability is controlled by factors such as lake–glacier proximity, lake morphology, topography, and atmospheric circulation in the model. Plateau-wide, the net lake effect emerges from the combined modulation of T_{2m}, snowfall, wind, and moisture transport.

Before interpreting these modeled patterns, it is important to consider model and observational limitations. Although the model exhibits noticeable seasonal biases in near-surface temperature and precipitation, part of these deviations likely arises from uncertainties in the reference datasets themselves. For instance, Wang et al. (2025) identified a systematic cold bias in ERA5 over the western TP, while the ERA-Interim dataset used for model initialization exhibits an even stronger cold bias, particularly over the Karakoram region. Similarly, satellite-derived precipitation estimates show considerable uncertainties in mountainous areas, with spatial and seasonal variations in accuracy (Zhang et al. 2023). Consequently, the validation results

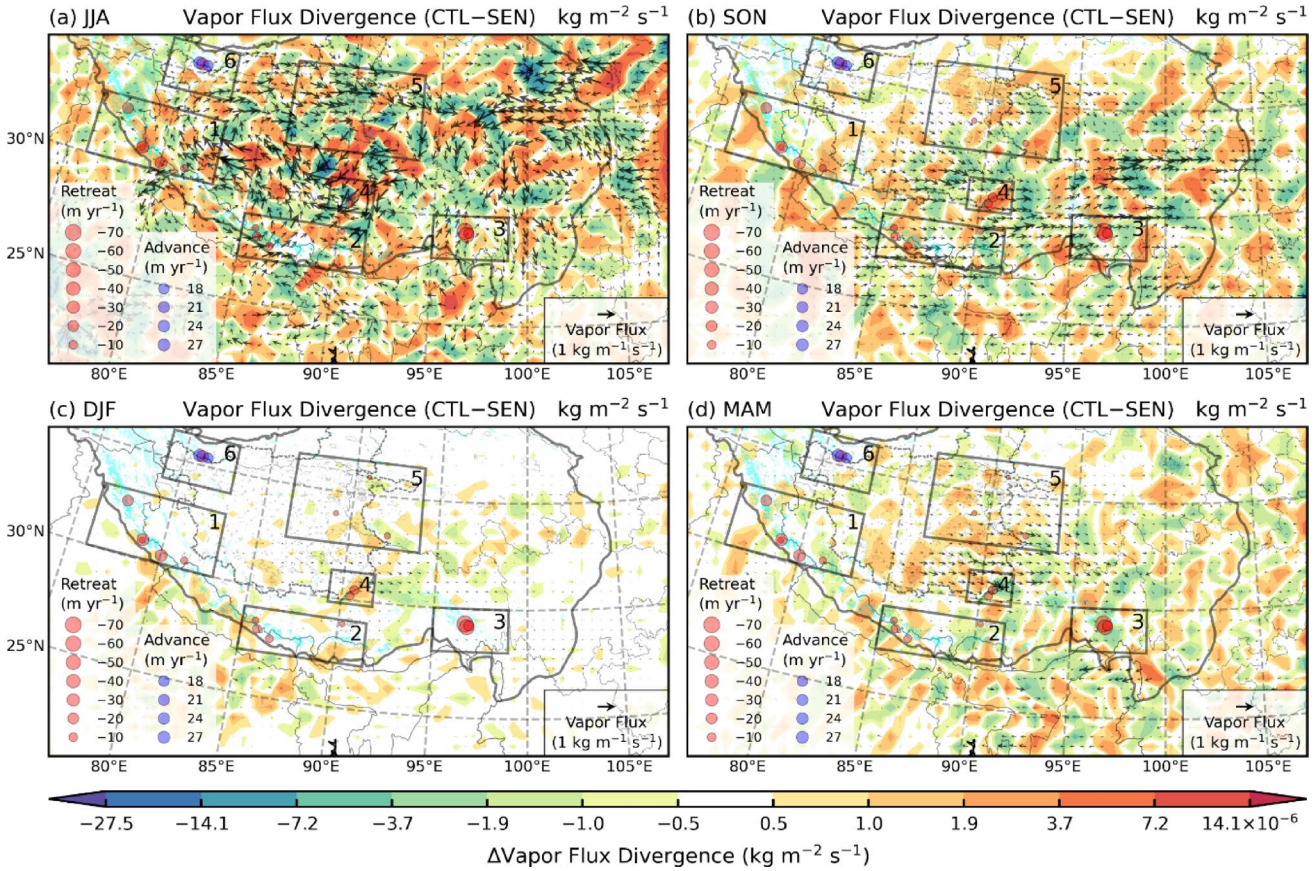

Fig. 12 The mean differences in simulated vapor flux (vectors, CTL−SEN; units: kg m^{-1} s^{-1}) and vapor flux divergence (color shading, CTL−SEN; units: × 10^{-6} kg m^{-2} s.$^{-1}$) between CTL and SEN experiments, vertically integrated from 500 to 200 hPa, during **a** summer (JJA), **b** autumn (SON), **c** winter(DJF), and **d** spring (MAM). Black boxes represent subregions 1−6. The solid black line delineates the TP, and the dashed black line outlines the Inner TP. The cyan areas show glacier distribution. Red (retreating) and blue (advancing) filled circles represent glaciers listed in Table 1, with circle sizes proportional to the rate of change as observed by Yao et al. (2012b)

provide qualitative guidance rather than a precise quantitative assessment. Since both experiments (with and without lakes) share identical boundary conditions and physical parameterizations, the differences between them primarily reflect the model's internal physical response to lake presence. Therefore, the present study focuses on elucidating the mechanisms of lake–atmosphere–glacier interactions and their regional–seasonal variability, rather than deriving quantitatively precise estimates of lake effects.

Within this context, our analysis reveals that TP lakes consistently exert a year-round cooling effect on surrounding land, with the strongest influence during summer, particularly across the lake-dense southern and eastern Inner TP. This cooling may generally suppress glacier ablation, especially for glaciers where summer T_{2m} approaches the melting point. However, both the magnitude and seasonal timing of lake-induced climatic effects vary regionally. Glaciers adjacent to major lakes, such as Naimona'nyi Glacier in the West Himalayas (near Langa Co and Mapam Yumco) and Qiangyong Glacier in the Central Himalayas (close to Yamzho Yumco and Puma Yumco), experience their most substantial lake influence in autumn. This is marked by pronounced simulated T_{2m} reductions (up to −2.5°C for Naimona'nyi) and enhanced snowfall (up to +26.4%), conditions that inhibit ablation and align with observed slow retreat rates (Brun et al. 2017; Yao et al. 2012b). The prominence of autumn signals in our simulations contrasts with previously reported winter/spring accumulation regimes for marginal Himalayan glaciers (Wang et al. 2017), suggesting that lake–atmosphere thermal contrasts in autumn may represent an additional modelled mechanism worth further study.

In the western Nyainqentanglha Range, the influence of Nam Co varies with slope aspect. Northern glaciers (e.g., Zhadang) benefit from summer cooling and increased winter-spring snowfall, while southern glaciers (e.g., Gurenhekou) are subject to autumn warming and reduced snowfall. This spatial divergence, driven by lake-induced wind divergence and convergence patterns, helps explain the contrasting retreat behaviors within the range (Luo et al. 2020). This mechanistic understanding extends earlier findings that emphasized only summer lake effects (Su et al. 2022b).

In the Tanggula Mountains, where glacier retreat is highly sensitive to summer warming under a continental climate (He et al. 2023; Zhang et al. 2018), the simulated warming effect of nearby lakes in summer and autumn (+0.20°C and +0.44°C at Xiaodongkemadi, respectively) emerges as a dominant negative influence, outweighing the minor benefits from cold-season snowfall. In contrast, glaciers in the high-altitude, thermally insensitive West Kunlun Mountains are more affected by simulated lake-induced snowfall increase, particularly during summer and autumn (+21.1% in autumn for Yulong Glacier). These increases are partly driven by lake-amplified northward moisture transport from the Indian Summer Monsoon into the northern TP, supporting the notion that precipitation variability sustains glacier mass balance in this region (de Kok et al. 2020; Kapnick et al. 2014). Further examination of regional circulation patterns reveals that TP lakes enhance summer monsoon moisture influx via the Himalayan valleys and facilitate clockwise transport along the Inner TP margins. This expanded vapor transport, combined with lake-evaporated moisture, results in increased snowfall over remote, high-altitude regions, such as the West Kunlun and Tanggula Mountains, partially accounting for the spatial heterogeneity in glacier response across the plateau (Farinotti et al. 2020).

A synthesis of the simulated lake-related influences points to regionally distinct mechanisms that could govern glacier response in the model, e.g., autumn cooling appears to limit ablation in some marginal Himalayan areas, while snowfall variability is a dominant pathway in the Inner TP, often modulated by T_{2m} differences due to slope orientation; in the West Kunlun, lake-induced enhancement of large-scale moisture transport and associated snowfall increases constitute the primary pathway through which lakes exert their climatic influence on glaciers. While prior studies emphasized summer effects (Su et al. 2022b), our findings identify autumn as the critical season for lake influence on marginal glaciers, owing to maximum lake-atmosphere thermal contrast and resulting dynamical responses.

Beyond spatial proximity, intrinsic physical features of TP lakes further modulate their climatic impact. Larger lakes such as Nam Co exert widespread cooling and moisture enhancement due to their high thermal inertia and strong evaporation, which reinforce lake–land thermal gradients and circulation feedbacks (Zhao et al. 2022b). Deep lakes like Mapam Yumco (70 m) and Puma Yumco (47 m) retain heat more efficiently, sustaining lake–atmosphere interactions well into late autumn before freezing up (Subin et al. 2012), corresponding to enhanced autumn snowfall observed in our simulations (Fig. 9d, Fig. 10d). High-altitude lakes such as Puma Yumco (~5,030 m) impose stronger localized effects due to their proximity to glacier accumulation zones and reduced atmospheric mixing, enhancing the spatial variability of cooling and snowfall patterns. Although seasonal or annual means tend to smooth short-term fluctuations, the error bars shown in Figs. 6 and 8 represent the 95% confidence intervals estimated via bootstrap resampling, indicating that the simulated lake effects remain significant despite uncertainty. This integrated perspective underscores that the climatic influence of TP lakes arises from complex thermal-dynamical interactions whose relative importance varies regionally and seasonally, shaped by lake characteristics, proximity, topography, and background climate.

Although our simulation covers only a single year (2013–2014), it captures typical large-scale features of the South Asian monsoon and winter westerlies, providing a representative backdrop for exploring lake-induced climatic influences on glacier-relevant variables (Huang et al. 2020; Singh et al. 2019). The study does not aim to explain long-term glacier change, but rather to elucidate how lake effects shape seasonal and spatial patterns in near-surface temperature and snowfall. Nonetheless, extrapolating our findings to longer timescales requires consideration of interannual variability, decadal climate modes, and glacier response timescales. Future studies incorporating multi-year simulations and dynamic glacier models are essential for assessing the long-term impacts of lake–glacier interactions.

6 Conclusions

In this study, the WRF-Lake model was employed to simulate the climatic effects of the TP lakes and their seasonal impacts on glacier behavior. Two sets of experiments were conducted: one with TP lakes and one without, to assess the climatic effects of TP lakes over the entire year, from June 2013 to May 2014. Both the seasonal climatic impacts of the TP lake cluster and individual lakes on glaciers were quantified.

The simulation results were first evaluated by comparing them with observational data. The findings suggest that the WRF-Lake model successfully reproduced the LSWT of two major TP lakes, Qinghai Lake and Nam Co, with BIAS values of 0.72 °C and 0.90 °C, and RMSE values of 2.08 °C and 2.10 °C, respectively. Overall, the model showed a reasonable ability to reproduce the broad spatial and temporal variability of T_{2m} and precipitation, consistent with previous studies over the TP, though regional discrepancies are still evident due to the complex topography and sparse observations.

The modelled climatic effects of TP lakes show seasonal variations. Many lakes produce cooling tendencies in spring and summer, and warming tendencies over lake surfaces in autumn and winter. Nevertheless, modeled T_{2m} over much

surrounding land often decreases in these experiments, which could locally reduce ablation under the simulated conditions. This effect appears to be particularly pronounced in the Inner TP, where most lakes are concentrated. In addition, TP lakes may significantly influence the distribution of snowfall in alpine regions, especially during summer and autumn, further impacting glacier dynamics.

Apart from the composite impact of the TP lakes, individual lakes may also exert more pronounced climatic effects on glaciers in their vicinity. For example, Langa Co and Mapam Yumco significantly reduce T_{2m} and increase snowfall over the Naimona'nyi Glacier to the south, contributing to the slowest retreat among glaciers in the West Himalayas. Similarly, Yamzho Yumco and Puma Yumco significantly lower T_{2m} and enhance snowfall over glaciers in their vicinity, including the Qiangyong Glacier, located to the west of the two lakes. These effects may help explain the relatively slower retreat of the Qiangyong Glacier among glaciers in the Central Himalayas. Nam Co, as the third-largest lake in the TP, may also exert a substantial impact on glaciers in the western Nyainqentanglha Range, particularly by influencing snowfall distribution and mitigating glacier ablation.

While this study provides simulated insights into lake–glacier interactions over the TP, several areas warrant further investigation and methodological improvement. First, adopting higher-resolution models and more sophisticated physical parameterizations could help resolve local-scale processes in complex glacier–lake terrains. Second, extending the analysis beyond a single year would enable better assessment of interannual variability linked to changing lake levels, monsoon dynamics, and westerly disturbances. Third, improving the representation of atmospheric processes and addressing data sparsity—particularly through expanded field observations—will enhance the fidelity of future simulations. Advancing these aspects through convection-permitting modeling, multi-year ensemble simulations, and improved lake–glacier coupling schemes will be key to deepening our understanding of glacier responses to evolving lake and climate conditions across the TP.

Acknowledgements We gratefully acknowledge the financial support provided by the National Natural Science Foundation of China (Grant Nos. 42305026, 42275044, and 42230610), the Major Science and Technology Project of Gansu Province (Grant No. 24ZD13FA003), and the Scientific Research Foundation of Chengdu University of Information Technology (Grant No. KYTZ202126). We sincerely thank the three anonymous reviewers for their constructive comments and insightful suggestions, which greatly improved the quality and clarity of this manuscript.

Author contributions DS conceptualized and led the manuscript writing, performed data analysis, and interpreted results. LW supervised the study design, provided strategic direction for experimental methodology, oversaw result interpretation, revised the manuscript for intellectual content, and approved the final version. AH and YW provided expertise in model simulations and validation. ML, XG, ZL, XY, and DJ assisted with data collection, model setup, and figure preparation. GK provided valuable feedback and guidance on the overall study design and manuscript. All authors participated in manuscript editing and approved the final version.

Funding This research was supported by the National Natural Science Foundation of China (Grant Nos. 42305026, 42275044, and 42230610), the Major Science and Technology Project of Gansu Province (Grant No. 24ZD13FA003), and the Scientific Research Foundation of Chengdu University of Information Technology (Grant No. KYTZ202126).

Data availability The ERA-Interim reanalysis dataset, ERA5-Land hourly dataset, and the Lake surface water temperature dataset used in this study are publicly accessible through the Copernicus Climate Data Store (CDS), available at https://cds.climate.copernicus.eu/. The IMERG daily precipitation data used in this study can be freely downloaded from https://pmm.nasa.gov/data-access/downloads/gpm.

Declarations

Competing interests The authors declare that they have no conflicts of interest.

References

Brun F, Berthier E, Wagnon P, Kaab A, Treichler D (2017) A spatially resolved estimate of High Mountain Asia glacier mass balances from 2000 to 2016. Nat Geosci 10:668. https://doi.org/10.1038/ngeo2999

Chen AA, Wang NL, Li Z, Wu YW, Zhang W, Guo ZM (2017) Region-wide glacier mass budgets for the Tanggula Mountains between similar to 1969 and similar to 2015 derived from remote sensing data. Arct Antarct Alp Res 49:551–568. https://doi.org/10.1657/aaar0016-065

Chen F, Dudhia J (2001) Coupling an advanced land surface-hydrology model with the Penn State-NCAR MM5 modeling system. Part II: preliminary model validation. Mon Weather Rev 129:587–604

Dai YF, Yao TD, Li XY, Ping F (2018) The impact of lake effects on the temporal and spatial distribution of precipitation in the Nam Co basin, Tibetan Plateau. Quat Int 475:63–69. https://doi.org/10.1016/j.quaint.2016.01.075

de Kok RJ, Kraaijenbrink PDA, Tuinenburg OA, Bonekamp PNJ, Immerzeel WW (2020) Towards understanding the pattern of glacier mass balances in High Mountain Asia using regional climatic modelling. Cryosphere 14:3215–3234. https://doi.org/10.5194/tc-14-3215-2020

de Kok RJ, Tuinenburg OA, Bonekamp PNJ, Immerzeel WW (2018) Irrigation as a potential driver for anomalous glacier behavior in High Mountain Asia. Geophys Res Lett 45:2047–2054. https://doi.org/10.1002/2017gl076158

Dee DP, Uppala SM, Simmons AJ, Berrisford P, Poli P, Kobayashi S, Andrae U, Balmaseda MA, Balsamo G, Bauer P, Bechtold P, Beljaars ACM, van de Berg L, Bidlot J, Bormann N, Delsol C, Dragani R, Fuentes M, Geer AJ, Haimberger L, Healy SB, Hersbach H, Hólm EV, Isaksen L, Kållberg P, Köhler M, Matricardi M, McNally AP, Monge-Sanz BM, Morcrette JJ, Park BK, Peubey C, de Rosnay P, Tavolato C, Thépaut JN, Vitart F (2011) The ERA-Interim reanalysis: configuration and performance of the data assimilation system. Q J R Meteorol Soc 137:553–597. https://doi.org/10.1002/qj.828

Donlon CJ, Minnett PJ, Gentemann C, Nightingale TJ, Barton IJ, Ward B, Murray MJ (2002) Toward improved validation of satellite sea surface skin temperature measurements for climate research. J Climate 15:353–369

Dudhia J (1989) Numerical study of convection observed during the winter monsoon experiment using a mesoscale two-dimensional model. J Atmos Sci 46:3077–3107

Farinotti D, Immerzeel WW, de Kok RJ, Quincey DJ, Dehecq A (2020) Manifestations and mechanisms of the Karakoram glacier anomaly. Nat Geosci 13:8. https://doi.org/10.1038/s41561-019-0513-5

Forsythe N, Fowler HJ, Li XF, Blenkinsop S, Pritchard D (2017) Karakoram temperature and glacial melt driven by regional atmospheric circulation variability. Nat Clim Chang 7:664. https://doi.org/10.1038/nclimate3361

Gilbert A, Leinss S, Kargel J, Kääb A, Gascoin S, Leonard G, Berthier E, Karki A, Yao T (2018) Mechanisms leading to the 2016 giant twin glacier collapses, Aru Range, Tibet. Cryosphere 12:2883–2900. https://doi.org/10.5194/tc-12-2883-2018

Grell GA, Devenyi D (2002) A generalized approach to parameterizing convection combining ensemble and data assimilation techniques. Geophys Res Lett 29(14):38–41. https://doi.org/10.1029/2002gl015311

Gu HP, Jin JM, Wu YH, Ek MB, Subin ZM (2015) Calibration and validation of lake surface temperature simulations with the coupled WRF-lake model. Clim Change 129:471–483. https://doi.org/10.1007/s10584-013-0978-y

He M, Li Z, Jiang W, Pan Y, Jiao J, Xiao Y (2023) Seasonal and interannual fluctuations of glacier mass balance and climate response processes on the Tibetan Plateau based on GRACE/GRACE-FO. IEEE Trans Geosci Remote Sens 61:1–9. https://doi.org/10.1109/tgrs.2023.3280714

Hewitt K (2005) The karakoram anomaly? Glacier expansion and the "elevation effect", Karakoram Himalaya. Mt Res Dev 25:332–340

Hong SY, Lim JOJ (2006) The WRF single-moment 6-class microphysics scheme (WSM6). Asia Pac J Atmos Sci 42:129–151

Hong SY, Noh Y, Dudhia J (2006) A new vertical diffusion package with an explicit treatment of entrainment processes. Mon Weather Rev 134:2318–2341. https://doi.org/10.1175/mwr3199.1

Hostetler SW, Bates GT, Giorgi F (1993) Interactive coupling of a lake thermal-model with a regional climate model. J Geophys Res-Atmos 98:5045–5057. https://doi.org/10.1029/92jd02843

Huang X, Zhou T, Turner A, Dai A, Chen X, Clark R, Jiang J, Man W, Murphy J, Rostron J, Wu B, Zhang L, Zhang W, Zou L (2020) The recent decline and recovery of Indian summer monsoon rainfall: relative roles of external forcing and internal variability. J Climate 33:5035–5060. https://doi.org/10.1175/jcli-d-19-0833.1

Hugonnet R, McNabb R, Berthier E, Menounos B, Nuth C, Girod L, Farinotti D, Huss M, Dussaillant I, Brun F, Kaab A (2021) Accelerated global glacier mass loss in the early twenty-first century. Nature 592:726–731. https://doi.org/10.1038/s41586-021-03436-z

Huss M, Hock R (2018) Global-scale hydrological response to future glacier mass loss. Nat Clim Chang 8:135–140. https://doi.org/10.1038/s41558-017-0049-x

Immerzeel WW, Lutz AF, Andrade M, Bahl A, Biemans H, Bolch T, Hyde S, Brumby S, Davies BJ, Elmore AC, Emmer A, Feng M, Fernndez A, Haritashya U, Kargel JS, Koppes M, Kraaijenbrink PDA, Kulkarni AV, Mayewski PA, Nepal S, Pacheco P, Painter TH, Pellicciotti F, Rajaram H, Rupper S, Sinisalo A, Shrestha AB, Viviroli D, Wada Y, Xiao C, Yao T, Baillie JEM (2020) Importance and vulnerability of the world's water towers. Nature 577:364. https://doi.org/10.1038/s41586-019-1822-y

Jouberton A, Shaw TE, Miles E, McCarthy M, Fugger S, Ren S, Dehecq A, Yang W, Pellicciotti F (2022) Warming-induced monsoon precipitation phase change intensifies glacier mass loss in the southeastern Tibetan Plateau. Proc Natl Acad Sci U S A 119:e2109796119. https://doi.org/10.1073/pnas.2109796119

Kääb A, Leinss S, Gilbert A, Bühler Y, Gascoin S, Evans SG, Bartelt P, Berthier E, Brun F, Chao W-A, Farinotti D, Gimbert F, Guo W, Huggel C, Kargel JS, Leonard GJ, Tian L, Treichler D, Yao T (2018) Massive collapse of two glaciers in western Tibet in 2016 after surge-like instability. Nat Geosci 11:114–120. https://doi.org/10.1038/s41561-017-0039-7

Kapnick SB, Delworth TL, Ashfaq M, Malyshev S, Milly PCD (2014) Snowfall less sensitive to warming in Karakoram than in Himalayas due to a unique seasonal cycle. Nat Geosci 7:834–840. https://doi.org/10.1038/Ngeo2269

Ke L, Song C (2014) Remotely sensed surface temperature variation of an inland saline lake over the central Qinghai-Tibet Plateau. ISPRS J Photogramm Remote Sens 98:157–167. https://doi.org/10.1016/j.isprsjprs.2014.09.007

Li X, O S, Wang N, Liu l, Huang Y (2021) Evaluation of the GPM IMERG V06 products for light rain over Mainland China. Atmos Res. https://doi.org/10.1016/j.atmosres.2021.105510

Li XF, Fowler HJ, Forsythe N, Blenkinsop S, Pritchard D (2018) The Karakoram/Western Tibetan vortex: seasonal and year-to-year variability. Climate Dyn 51:3883–3906. https://doi.org/10.1007/s00382-018-4118-2

Li XY, Ma YJ, Huang YM, Hu X, Wu XC, Wang P, Li GY, Zhang SY, Wu HW, Jiang ZY, Cui BL, Liu L (2016) Evaporation and surface energy budget over the largest high-altitude saline lake on the Qinghai-Tibet Plateau. J Geophys Res-Atmos 121:10470–10485. https://doi.org/10.1002/2016jd025027

Li Y, Wang C, Huang R, Yan D, Peng H, Xiao S (2022) Spatial distribution of oceanic moisture contributions to precipitation over the Tibetan Plateau. Hydrol Earth Syst Sci 26:6413–6426. https://doi.org/10.5194/hess-26-6413-2022

Li Z, Lyu S, Wen L, Zhao L, Ao Y, Wang S (2017) Effect of a cold, dry air incursion on atmospheric boundary layer processes over a high-altitude lake in the Tibetan Plateau. Atmos Res 185:32–43. https://doi.org/10.1016/j.atmosres.2016.10.024

Luo W, Zhang GQ, Chen WF, Xu FL (2020) Response of glacial lakes to glacier and climate changes in the western Nyainqentanglha range. Sci Total Environ 735:10. https://doi.org/10.1016/j.scitotenv.2020.139607

Maussion F, Scherer D, Molg T, Collier E, Curio J, Finkelnburg R (2014) Precipitation seasonality and variability over the Tibetan Plateau as resolved by the high asia reanalysis. J Climate 27:1910–1927. https://doi.org/10.1175/jcli-d-13-00282.1

Meng X, Lyu S, Zhang T, Zhao L, Li Z, Han B, Li S, Ma D, Chen H, Ao Y, Luo S, Shen Y, Guo J, Wen L (2018) Simulated cold bias being improved by using MODIS time-varying albedo in the Tibetan Plateau in WRF model. Environ Res Lett 13(4):044028. https://doi.org/10.1088/1748-9326/aab44a

Miao C, Immerzeel WW, Xu B, Yang K, Duan Q, Li X (2024) Understanding the Asian water tower requires a redesigned precipitation observation strategy. Proce Natl Acad Sci 121(23):e2403557121. https://doi.org/10.1073/pnas.2403557121

Miles E, McCarthy M, Dehecq A, Kneib M, Fugger S, Pellicciotti F (2021) Health and sustainability of glaciers in High Mountain Asia. Nat Commun 12(1):2868. https://doi.org/10.1038/s41467-021-23073-4

Mlawer EJ, Taubman SJ, Brown PD, Iacono MJ, Clough SA (1997) Radiative transfer for inhomogeneous atmospheres: RRTM, a validated correlated-k model for the longwave. J Geophys Res Atmos 102:16663–16682. https://doi.org/10.1029/97jd00237

Muñoz-Sabater J, Dutra E, Agustí-Panareda A, Albergel C, Arduini G, Balsamo G, Boussetta S, Choulga M, Harrigan S, Hersbach H, Martens B, Miralles DG, Piles M, Rodríguez-Fernández NJ, Zsoter E, Buontempo C, Thépaut J-N (2021) ERA5-land: a state-of-the-art global reanalysis dataset for land applications. Earth

Syst Sci Data 13:4349–4383. https://doi.org/10.5194/essd-13-4349-2021

Politi E, Maccallum S, Cutler MEJ, Merchant CJ, Rowan JS, Dawson TP (2016) Selection of a network of large lakes and reservoirs suitable for global environmental change analysis using Earth Observation. Int J Remote Sens 37:3042–3060. https://doi.org/10.1080/01431161.2016.1192702

Qiu J (2008) China: the third pole. Nature 454:393–396. https://doi.org/10.1038/454393a

Rounce DR, Hock R, Maussion F, Hugonnet R, Kochtitzky W, Huss M, Berthier E, Brinkerhoff D, Compagno L, Copland L, Farinotti D, Menounos B, McNabb RW (2023) Global glacier change in the 21st century: every increase in temperature matters. Science 379:78–83. https://doi.org/10.1126/science.abo1324

Sakai A, Fujita K (2017) Contrasting glacier responses to recent climate change in high-mountain Asia. Sci Rep 7:8. https://doi.org/10.1038/s41598-017-14256-5

Shaw TE, Miles ES, Chen D, Jouberton A, Kneib M, Fugger S, Ou T, Lai HW, Fujita K, Yang W, Fatichi S, Pellicciotti F (2022) Multi-decadal monsoon characteristics and glacier response in High Mountain Asia. Environ Res Lett 17(10):104001. https://doi.org/10.1088/1748-9326/ac9008

Singh D, Ghosh S, Roxy MK, McDermid S (2019) Indian summer monsoon: extreme events, historical changes, and role of anthropogenic forcings. Wires Clim Change 10(2):e571. https://doi.org/10.1002/wcc.571

Skamarock WC, Klemp JB, Dudhia J, Gill DO, Barker DM, Wang W, Powers JG (2008) A description of the advanced research WRF version 3. NCAR Technical note-475+ STR.

Su B, Xiao C, Chen D, Huang Y, Che Y, Zhao H, Zou M, Guo R, Wang X, Li X, Guo W, Liu S, Yao T (2022a) Glacier change in China over past decades: Spatiotemporal patterns and influencing factors. Earth-Sci Rev 226:103926. https://doi.org/10.1016/j.earscirev.2022.103926

Su DS, Wen LJ, Gao XQ, Lepparanta M, Song XY, Shi QQ, Kirillin G (2020) Effects of the largest lake of the Tibetan Plateau on the regional climate. j Geophys Res Atmos 125(22):e2020JD033396. https://doi.org/10.1029/2020JD033396

Su DS, Wen LJ, Huang AN, Wu Y, Gao XQ, Wang MX, Zhao YX, Kirillin G (2022b) Simulation of the potential impacts of lakes on glacier behavior over the Tibetan Plateau in summer. Clim Dyn. https://doi.org/10.1007/s00382-022-06517-5

Subin ZM, Riley WJ (2001) Mironov D (2012) An improved lake model for climate simulations: model structure, evaluation, and sensitivity analyses in CESM1. J Adv Model Earth Syst 4:1. https://doi.org/10.1029/2011ms000072

Thiebaux J, Rogers E, Wang WQ, Katz B (2003) A new high-resolution blended real-time global sea surface temperature analysis. Bull Am Meteorol Soc 84:645. https://doi.org/10.1175/bams-84-5-645

Thiery W, Davin EL, Panitz HJ, Demuzere M, Lhermitte S, van Lipzig N (2015) The impact of the African Great Lakes on the regional climate. J Climate 28:4061–4085. https://doi.org/10.1175/Jcli-D-14-00565.1

van Angelen JH, M. Lenaerts JT, van den Broeke MR, Fettweis X, van Meijgaard E (2013) Rapid loss of firn pore space accelerates 21st century Greenland mass loss. Geophys Res Lett 40:2109–2113. https://doi.org/10.1002/grl.50490

van Pelt Wjj, Pohjola VA, Reijmer CH (2016) The changing impact of snow conditions and refreezing on the mass balance of an idealized Svalbard Glacier. Front Earth Sci 4:15. https://doi.org/10.3389/feart.2016.00102

Wang J, Li XF, Wang JZ, Lai X, Yang S, Forsythe N, Fowler HJ (2025) Evaluation of reanalyzed surface air temperature over the western Tibetan Plateau. Atmos Res 329:108454

Wang P, Li Z, Li H, Zhang Z, Xu L, Yue X (2020) Glaciers in Xinjiang, China: past changes and current status. Water 12(9):2367. https://doi.org/10.3390/w12092367

Wang QY, Yi S, Chang L, Sun WK (2017) Large-scale seasonal changes in glacier thickness across High Mountain Asia. Geophys Res Lett 44:10427–10435. https://doi.org/10.1002/2017gl075300

Wen L, Lv S, Li Z, Zhao L, Nagabhatla N (2015) Impacts of the two biggest lakes on local temperature and precipitation in the Yellow River Source Region of the Tibetan Plateau. Adv Meteorol 2015:248031. https://doi.org/10.1155/2015/248031

Wu Y, Huang AN, Yang B, Dong GT, Wen LJ, Lazhu ZZQ, Fu ZP, Zhu XY, Zhang XD, Cai SX (2019) Numerical study on the climatic effect of the lake clusters over Tibetan Plateau in summer. Clim Dyn 53:5215–5236. https://doi.org/10.1007/s00382-019-04856-4

Yang K, Wu H, Qin J, Lin CG, Tang WJ, Chen YY (2014) Recent climate changes over the Tibetan Plateau and their impacts on energy and water cycle: a review. Glob Planet Change 112:79–91. https://doi.org/10.1016/j.gloplacha.2013.12.001

Yang MX, Wang XJ, Pang GJ, Wang GN, Liu ZC (2019) The Tibetan Plateau cryosphere: observations and model simulations for current status and recent changes. Earth-Sci Rev 190:353–369. https://doi.org/10.1016/j.earscirev.2018.12.018

Yao T, Bolch T, Chen D, Gao J, Immerzeel W, Piao S, Su F, Thompson L, Wada Y, Wang L, Wang T, Wu G, Xu B, Yang W, Zhang G, Zhao P (2022) The imbalance of the Asian water tower. Nature Rev Earth Environ 3:618–632. https://doi.org/10.1038/s43017-022-00299-4

Yao TD, Thompson L, Mosbrugger V, Zhang F, Ma YM, Luo TX, Xu BQ, Yang XX, Joswiak DR, Wang WC, Joswiak M, Devkota LP, Tayal S, Jilani R, Fayziev R (2012a) Third pole environment (TPE). Environ Dev 3:52–64. https://doi.org/10.1016/j.envdev.2012.04.002

Yao TD, Thompson L, Yang W, Yu WS, Gao Y, Guo XJ, Yang XX, Duan KQ, Zhao HB, Xu BQ, Pu JC, Lu AX, Xiang Y, Kattel DB, Joswiak D (2012b) Different glacier status with atmospheric circulations in Tibetan Plateau and surroundings. Nat Clim Chang 2:663–667. https://doi.org/10.1038/Nclimate1580

Yao TD, Xue YK, Chen DL, Chen FH, Thompson L, Cui P, Koike T, Lau WKM, Lettenmaier D, Mosbrugger V, Zhang RH, Xu BQ, Dozier J, Gillespie T, Gu Y, Kang SC, Piao SL, Sugimoto S, Ueno K, Wang L, Wang WC, Zhang F, Sheng YW, Guo WD, Ailikun YXX, Ma YM, Shen SSP, Su ZB, Chen F, Liang SL, Liu YM, Singh VP, Yang K, Yang DQ, Zhao XQ, Qian Y, Zhang Y, Li Q (2019) Recent third pole's rapid warming accompanies cryospheric melt and water cycle intensification and interactions between monsoon and environment: multidisciplinary approach with observations, modeling, and analysis. Bull Am Meteor Soc 100:423–444. https://doi.org/10.1175/bams-d-17-0057.1

Yao XN, Yang K, Zhou X, Wang Y, Lazhu CYY, Lu H (2021) Surface friction contrast between water body and land enhances precipitation downwind of a large lake in Tibet. Clim Dyn. https://doi.org/10.1007/s00382-020-05575-x

Yu WS, Yao TD, Kang SC, Pu JC, Yang W, Gao TG, Zhao HB, Zhou H, Li SH, Wang WC, Ma LL (2013) Different region climate regimes and topography affect the changes in area and mass balance of glaciers on the north and south slopes of the same glacierized massif (the West Nyainqentanglha Range, Tibetan Plateau). J Hydrol 495:64–73. https://doi.org/10.1016/j.jhydrol.2013.04.034

Zhang GQ, Yao TD, Chen WF, Zheng GX, Shum CK, Yang K, Piao SL, Sheng YW, Yi S, Li JL, O'Reilly CM, Qi SH, Shen SSP, Zhang HB, Jia YY (2019) Regional differences of lake evolution across China during 1960s–2015 and its natural and anthropogenic causes. Remote Sens Environ 221:386–404. https://doi.org/10.1016/j.rse.2018.11.038

Zhang H, Immerzeel WW, Zhang F, de Kok RJ, Chen D, Yan W (2022) Snow cover persistence reverses the altitudinal patterns of warming above and below 5000 m on the Tibetan Plateau. Sci Total Environ. https://doi.org/10.1016/j.scitotenv.2021.149889

Zhang W, Di Z, Liu J, Zhang S, Liu Z, Wang X, Sun H (2023) Evaluation of five satellite-based precipitation products for extreme rainfall estimations over the qinghai-tibet plateau. Remote Sens 15(22):5379. https://doi.org/10.3390/rs15225379

Zhang ZM, Jiang LM, Liu L, Sun YF, Wang HS (2018) Annual glacier-wide mass balance (2000–2016) of the interior tibetan plateau reconstructed from MODIS albedo products. Remote Sens 10(7):1031. https://doi.org/10.3390/rs10071031

Zhao F, Long D, Li X, Huang Q, Han P (2022a) Rapid glacier mass loss in the Southeastern Tibetan Plateau since the year 2000 from satellite observations. Remote Sens Environ 270:112853. https://doi.org/10.1016/j.rse.2021.112853

Zhao Z, Huang A, Ma W, Wu Y, Wen L, Lazhu GuC (2022b) Effects of Lake Nam Co and surrounding terrain on extreme precipitation over nam co basin tibetan plateau a case study. J Geophys Res Atmos 127(10):e2021JD036190. https://doi.org/10.1029/2021jd036190

Zhu L, Jin J, Liu Y (2020) Modeling the effects of lakes in the Tibetan Plateau on diurnal variations of regional climate and their seasonality. J Hydrometeorol 21:2523–2536. https://doi.org/10.1175/jhm-d-20-0091.1

Zhu ML, Yao TD, Yang W, Xu BQ, Wu GJ, Wang XJ (2017) Differences in mass balance behavior for three glaciers from different climatic regions on the Tibetan Plateau. Clim Dyn 50:3457–3484. https://doi.org/10.1007/s00382-017-3817-4

Terms and Conditions

Springer Nature journal content, brought to you courtesy of Springer Nature Customer Service Center GmbH (“Springer Nature”).
Springer Nature supports a reasonable amount of sharing of research papers by authors, subscribers and authorised users (“Users”), for small-scale personal, non-commercial use provided that all copyright, trade and service marks and other proprietary notices are maintained. By accessing, sharing, receiving or otherwise using the Springer Nature journal content you agree to these terms of use (“Terms”). For these purposes, Springer Nature considers academic use (by researchers and students) to be non-commercial.
These Terms are supplementary and will apply in addition to any applicable website terms and conditions, a relevant site licence or a personal subscription. These Terms will prevail over any conflict or ambiguity with regards to the relevant terms, a site licence or a personal subscription (to the extent of the conflict or ambiguity only). For Creative Commons-licensed articles, the terms of the Creative Commons license used will apply.
We collect and use personal data to provide access to the Springer Nature journal content. We may also use these personal data internally within ResearchGate and Springer Nature and as agreed share it, in an anonymised way, for purposes of tracking, analysis and reporting. We will not otherwise disclose your personal data outside the ResearchGate or the Springer Nature group of companies unless we have your permission as detailed in the Privacy Policy.
While Users may use the Springer Nature journal content for small scale, personal non-commercial use, it is important to note that Users may not:

1. use such content for the purpose of providing other users with access on a regular or large scale basis or as a means to circumvent access control;
2. use such content where to do so would be considered a criminal or statutory offence in any jurisdiction, or gives rise to civil liability, or is otherwise unlawful;
3. falsely or misleadingly imply or suggest endorsement, approval , sponsorship, or association unless explicitly agreed to by Springer Nature in writing;
4. use bots or other automated methods to access the content or redirect messages
5. override any security feature or exclusionary protocol; or
6. share the content in order to create substitute for Springer Nature products or services or a systematic database of Springer Nature journal content.

In line with the restriction against commercial use, Springer Nature does not permit the creation of a product or service that creates revenue, royalties, rent or income from our content or its inclusion as part of a paid for service or for other commercial gain. Springer Nature journal content cannot be used for inter-library loans and librarians may not upload Springer Nature journal content on a large scale into their, or any other, institutional repository.
These terms of use are reviewed regularly and may be amended at any time. Springer Nature is not obligated to publish any information or content on this website and may remove it or features or functionality at our sole discretion, at any time with or without notice. Springer Nature may revoke this licence to you at any time and remove access to any copies of the Springer Nature journal content which have been saved.
To the fullest extent permitted by law, Springer Nature makes no warranties, representations or guarantees to Users, either express or implied with respect to the Springer nature journal content and all parties disclaim and waive any implied warranties or warranties imposed by law, including merchantability or fitness for any particular purpose.
Please note that these rights do not automatically extend to content, data or other material published by Springer Nature that may be licensed from third parties.
If you would like to use or distribute our Springer Nature journal content to a wider audience or on a regular basis or in any other manner not expressly permitted by these Terms, please contact Springer Nature at

onlineservice@springernature.com